

A TRANSNUCLEAR CALCULATION PACKAGE

PAGE: 1 of 64

CALCULATION NO: SCE-23.0410 NP PROJECT NAME: San Onofre Unit 2/3 Dry Cask Storage

PROJECT NO: SCE-23 CLIENT: Southern California Edison

CALCULATION TITLE:

Thermal Analysis of NUHOMS® Advanced Horizontal Storage Module Using CFD Method

SUMMARY DESCRIPTION:

The NUHOMS® Advanced Horizontal Storage Module (AHSM) is a concrete structure used to house dry shielded canisters (DSCs) containing spent nuclear fuel assemblies. This calculation provides an evaluation of the thermal performance of the AHSM for the bounding design basis ambient condition using a computational fluid dynamics (CFD) methodology. The CFD methodology used for this analysis has been validated against full scale test data for the NUHOMS® 07P HSM.

**NON-PROPRIETARY
FOR INFORMATION ONLY**

REVISION	TOTAL PAGES AND DISKS (IF ANY)	NAMES AND INITIALS OF PREPARERS & DATES	NAMES AND INITIALS OF VERIFIERS & DATES	APPROVER NAME AND SIGNATURE	APPROVAL DATE
0	45 + A1 + B1 to B27 1 CD	Gregory J. Banken	Larry H. Nielsen	Ian McInnes	1/07/04
1	47 + A1 1 CD	Gregory J. Banken	Marcel D. Berz	Ian McInnes	6/22/04
2	64 + A1	Gregory J. Banken <i>Gregory Banken</i> 6/28/04	Marcel D. Berz <i>Marcel D. Berz</i> 6/28/04	<i>Ian McInnes</i> <i>A</i>	6/30/04

A TRANSNUCLEAR

PROJECT NO: SCE-23	REVISION: 2
CALCULATION NO: SCE-23.0410	PAGE: 2 of 65

REVISION SUMMARY

REV.	DATE	DESCRIPTION	AFFECTED PAGES	AFFECTED DISKS
0	1/07/04	Initial Release	ALL	N/A
1	6/22/04	Convert calculation from confirmatory to design basis analysis, revised DSC modeling approach to account for surface-to-surface radiation methodology, use second order discretization solution technique, moved analysis of NUHOMS 7P HSM to standalone V&V calculation, and switched ambient condition used for the analysis from off-normal normal summer storage condition since the normal summer storage condition has the lowest thermal margin for the fuel cladding.	1-8, 10-18, 20, 22-47, A1	
2	6/30/04	Add analysis for off-normal cold (-40°F) ambient condition and provide editorial pickups.	1-7, 13-14, 16, 17, 28-63, A1	

A TRANSNUCLEAR

PROJECT NO: SCE-23	REVISION: 2
CALCULATION NO: SCE-23.0410	PAGE: 3 of 65

TABLE OF CONTENTS

	<u>Page</u>
1. INTRODUCTION.....	6
1.1 Objective	6
1.2 Purpose of Revision 0.....	6
1.3 Purpose of Revision 1.....	6
1.4 Purpose of Revision 2.....	6
1.5 Scope	6
2. ASSUMPTIONS AND CONSERVATISMS	6
2.1 General Assumptions	6
2.2 Conservatisms	7
3. AHSM DESIGN.....	7
3.1 AHSM Geometry	7
3.2 Material Properties	8
4. CALCULATIONS	13
4.1 Fluent™/ Icepak™ Model.....	13
4.2 Thermal Analysis at Bounding Design Basis Ambient Condition.....	16
4.3 Thermal Analysis at Off-Normal Cold Ambient Condition.....	45
5. SUMMARY AND CONCLUSION.....	59
6. REFERENCES.....	64
 APPENDIX A: FLUENT™ / ICEPAK™ RUN LOG.....	 A1

A TRANSNUCLEAR

PROJECT NO: SCE-23	REVISION: 2
CALCULATION NO: SCE-23.0410	PAGE: 4 of 65

LIST OF TABLES

	<u>Page</u>
Table 3-1 - Material Properties, Solids.....	9
Table 3-2 - Material Properties, Air	9
Table 5-1 - Summary of Peak Component Temperatures For Normal Hot Storage	61
Table 5-2 - Summary of Peak Component Temperatures For Off-Normal Cold Storage.....	62
Table 5-3 - DSC Shell Temperatures vs. Circumferential Position	63
Table A-1 - FLUENT™ / ICEPAK™ Run Log.....	1

LIST OF FIGURES

	<u>Page</u>
Figure 3-1 - Illustration of Typical NUHOMS AHSM Storage Array	10
Figure 3-2 - Cross-Section View Through Center Of AHSM Module	11
Figure 3-3 - View Of DSC Support Structure & Heat Shields.....	12
Figure 4-1 - Isometric, Wireframe View Of Model Layout	19
Figure 4-2 - Cutaway View #1 Of Module Base Unit Model	20
Figure 4-3 - Cutaway View #2 Of Module Base Unit Model	21
Figure 4-4 - View Of Inlet Duct For Module Base	22
Figure 4-5 - Isometric View Of Seven (7) Segments Used To Simulate DSC Within Module.....	23
Figure 4-6 - Isometric View Of DSC & Heat Shield Layout Within Model.....	24
Figure 4-7 - Perspective View Of Meshing At X-Y Plane Of AHSM	25
Figure 4-8 - Enlarged View Of Meshing At DSC Support Structure.....	26
Figure 4-9 - Elevation View Of Meshing At Z-Y Plane Of AHSM.....	27
Figure 4-10 - Temperature Distribution On DSC Surface, Perspective View, Normal Hot Storage Condition	28
Figure 4-11 - Temperature Distribution On DSC, Side View, Normal Hot Storage Condition	29
Figure 4-12 - Temperature Distribution On DSC, Bottom View, Normal Hot Storage Condition.....	30
Figure 4-13 - Temperature Distribution On Heat Shield Surfaces, Normal Hot Storage Condition	31
Figure 4-14 - Elevation View Of Temperature Distribution On Heat Shield, Normal Hot Storage Condition	32
Figure 4-15 - Temperature Distribution On Concrete Surfaces Of Base Unit, Normal Hot Storage Condition	33
Figure 4-16 - Temperature Distribution On Concrete Vault Surfaces, Normal Hot Storage Condition	34
Figure 4-17 - Module Centerline Temperature Profile, Including Airspace, Normal Hot Storage Condition	35
Figure 4-18 - Temperature Variation at Exhaust Vent, Normal Hot Storage Condition	36
Figure 4-19 - Velocity Variation at Exhaust Vent, Normal Hot Storage Condition	36
Figure 4-20 - Velocity Profile Along X-Y Plane Through AHSM, Normal Hot Storage Condition	37

A TRANSNUCLEAR

PROJECT NO: SCE-23	REVISION: 2
CALCULATION NO: SCE-23.0410	PAGE: 5 of 65

Figure 4-21 - Velocity Profile Along X-Y Plane Midway Through AHSM, Normal Hot Storage Condition	38
Figure 4-22 - Velocity Profile Along X-Y Plane Through AHSM, Normal Hot Storage Condition	39
Figure 4-23 - Velocity Profile Along X-Y Plane In Vicinity Of DSC Support Structure, Normal Hot Storage Condition	40
Figure 4-24 - Velocity Profile Along X-Y Plane In Vicinity Of Front Vault Duct, Normal Hot Storage Condition	41
Figure 4-25 - Velocity Profile Along Y-Z Plane At Center Of AHSM, Normal Hot Storage Condition	42
Figure 4-26 - Velocity Profile Along Y-Z Plane In Vicinity Of Vault Roof Ducts, Normal Hot Storage Condition	43
Figure 4-27 - Velocity Profile Along Y-Z Plane Approximately 22" From Edge Of AHSM, Normal Hot Storage Condition	44
Figure 4-28 - Temperature Distribution On DSC Surface, Perspective View, Off-Normal Cold Storage Condition	47
Figure 4-29 - Temperature Distribution On DSC, Side View, Off-Normal Cold Storage Condition	48
Figure 4-30 - Temperature Distribution On DSC, Bottom View, Off-Normal Cold Storage Condition	49
Figure 4-31 - Temperature Distribution On Heat Shield Surfaces, Off-Normal Cold Storage Condition	50
Figure 4-32 - Elevation View Of Temperature Distribution On Heat Shield, Off-Normal Cold Storage Condition	51
Figure 4-33 - Temperature Distribution On Concrete Surfaces Of Base Unit, Off-Normal Cold Storage Condition	52
Figure 4-34 - Temperature Distribution On Concrete Vault Surfaces, Off-Normal Cold Storage Condition	53
Figure 4-35 - Module Centerline Temperature Profile, Including Airspace, Off-Normal Cold Storage Condition	54
Figure 4-36 - Temperature Variation at Exhaust Vent, Off-Normal Cold Storage Condition	55
Figure 4-37 - Velocity Variation at Exhaust Vent, Off-Normal Cold Storage Condition	55
Figure 4-38 - Velocity Profile Along X-Y Plane Through AHSM, Off-Normal Cold Storage Condition	56
Figure 4-39 - Velocity Profile Along X-Y Plane Through AHSM, Off-Normal Cold Storage Condition	57
Figure 4-40 - Velocity Profile Along Y-Z Plane At Center Of AHSM, Off-Normal Cold Storage Condition	58

PROJECT NO: SCE-23	REVISION: 2
CALCULATION NO: SCE-23.0410	PAGE: 6 of 65

1. INTRODUCTION

1.1 Objective

The objective of this calculation is to analyze the thermal performance for the NUHOMS[®] Advanced Horizontal Storage Module (AHSM) under the bounding design basis condition of storage. The bounding condition of storage is the normal summer condition with a peak 104°F ambient air temperature, 24-hour averaged insolation loading, and with an internal DSC decay heat loading of 24 kW. This condition yields the lowest thermal margin for the predicted fuel cladding temperature. The evaluation is conducted as a steady-state analysis using a computational fluid dynamics (CFD) methodology to directly calculate the prototypical flow regime within the AHSM.

1.2 Purpose of Revision 0

The thermal performance of the NUHOMS[®] AHSM design was evaluated using a combination of computer modeling (i.e., HEATING7) and hand calculations. The purpose of Revision 0 to the calculation was to perform an independent, confirmatory analysis of the thermal performance of the AHSM for one thermal condition using an alternative methodology.

1.3 Purpose of Revision 1

The purpose of Revision 1 was to create a design basis CFD model of the AHSM and to evaluate the thermal performance of the AHSM for the bounding design basis condition of storage.

1.4 Purpose of Revision 2

The purpose of Revision 2 is to add an evaluation of the thermal performance of the AHSM for the off-normal cold condition of storage (i.e., -40°F ambient without insolation). This condition is evaluated as a potential bounding case for thermal gradients in the AHSM.

1.5 Scope

The scope of this calculation is limited to the NUHOMS[®] AHSM design, as defined by its design drawings [6.2], and for storage conditions with a peak ambient air temperature of 104°F or less, 24-hour averaged insolation loading, and with an internal DSC decay heat loading of 24 kW or less.

2. ASSUMPTIONS AND CONSERVATISMS

2.1 General Assumptions

- 2.1.1 The design basis ambient condition used for this calculation is the normal hot storage condition with a daily maximum ambient air temperature of 104°F. Per the [6.1] analyses, a steady-state, 24-hour average ambient temperature of 97°F will bound the transient thermal performance of the AHSM module over the daily ambient temperature range. Evaluation of the thermal performance at the off-normal cold storage condition

A TRANSCLEAR

PROJECT NO: SCE-23	REVISION: 2
CALCULATION NO: SCE-23.0410	PAGE: 7 of 65

with an ambient air temperature of -40°F and no insolation will establish the maximum thermal gradients expected in the AHSM.

- 2.1.2 The geometry of the NUHOMS[®] AHSM is defined by the [6.2] design drawings.
- 2.1.3 The design decay heat loading for the AHSM is 24 kW. It is assumed that the heat loading is equally distributed over the active fuel length of 150" for the CE 16x16 fuel assemblies (FAs). The active fuel region is assumed to begin 4" above the bottom shield plug.
- 2.1.4 The analysis is based on a 24PT4 DSC with an outer diameter of 67.19" and a maximum length of 196.3". The bottom shield plug assembly has a minimum thickness of 6.75", while the top shield plug assembly and outer cover plate have a combined minimum thickness of 8.07". The minimum canister cavity length is 180.2" between the top and bottom shield plugs. The front of the DSC begins 7.25" from the inside, front wall of the AHSM.
- 2.1.5 The analysis conservatively assumes the AHSM is located within array of AHSM modules. As such, solar loading for the normal hot storage condition is applied only to the roof and front face of the AHSM. Per the [6.1] analyses, the 24-hour average insolation on the roof is $0.852 \text{ Btu/hr-in}^2$ or $122.7 \text{ Btu/hr-ft}^2$, while the 24-hour average insolation on the front face is $0.213 \text{ Btu/hr-in}^2$ or 30.7 Btu/hr-ft^2 . Zero insolation is assumed for the off-normal cold storage condition.

2.2 Conservatism

- 2.2.1 For simplicity and conservatism, the approximately 17 inches of additional stack height (8.5 inches to the mean height) represented by the roof shield cap over the exit opening is conservatively ignored. However, the loss factors associated with the flow turn and screened opening are included as a flow resistance element in the modeling.
- 2.2.2 The vertical flow channel at the back of the AHSM leading to the roof vent cap, together with the vent cap and outlet screen, are modeled 16" narrower than the actual width to simplify the meshing in that region. As such, the exit velocities will be approximately 20% higher for the same airflow rate.

3. AHSM DESIGN

3.1 AHSM Geometry

Figure 3-1 illustrates the typical AHSM storage array. In the typical arrangement, the modules are placed side-by-side and back-to-back to conserve ground space and maximize self-shielding. This arrangement results in only the top and front faces of the interior modules being exposed to the ambient, while the sides and back surfaces are essentially adiabatic surfaces (i.e., no heat transfer across the boundary). The airflow path through the AHSM starts by the air being drawn in through the screened opening at the front face of the module, travels through the z-shaped duct (see Figure

A

TRANSNUCLEAR

PROJECT NO: SCE-23	REVISION: 2
CALCULATION NO: SCE-23.0410	PAGE: 8 of 65

3-2), before entering the plenum space below the DSC. Once in the plenum space, the air flows upward around the DSC and on both the sides of the heat shields before passing into the two vertical air ducts at the top of the module vault. After exiting the vertical air ducts, the airflow turns horizontal and flows under the concrete roof slab to the back of the module, turns vertical again and flows upward before making a final turn and exiting the module at the screened opening.

Figure 3-1 and Figure 3-2 illustrate the overall layout and dimensioning of the module's base unit, while Figure 3-3 illustrates an elevation view of the module's interior and the DSC support structure. The support rails are W10x12 wide flanges with Nitronic rub strips.

3.2 Material Properties

The material properties used for this analysis are taken from the [6.1] calculation. Table 3-1 presents the material properties assumed for the concrete, the Type 304 stainless steel used for the DSC shell and the heat shields, and the carbon steel used for the DSC support structure. Fixed specific heat values are used for the various materials for simplicity and since the value of specific heat has no impact in a steady-state calculation. Fixed values for thermal conductivity are also used for the soil and carbon steel given the limited change with temperature and the minor impact these materials have on the thermal performance of the module. The soil below the base mat of the AHSM module is assumed to have a constant earth temperature of 70°F.

The temperature dependant thermal properties used for air [6.9] are presented in Table 3-2.

A TRANSNUCLEAR

PROJECT NO: SCE-23	REVISION: 2
CALCULATION NO: SCE-23.0410	PAGE: 9 of 65

Table 3-1 - Material Properties, Solids

Material	Temperature °F	Density lbm/ft ³	Specific Heat Btu/lbm-°F	Conductivity Btu/hr-ft-°F	Emissivity
Concrete	0	145	0.25	0.917	0.9
	100			1.17	
	200			1.14	
	500			1.04	
	1000			0.80	
Soil	---	128	0.44	0.30	---
Carbon Steel	---	489	0.12 ¹	24.4	0.85 for painted support structure
Type 304 Stainless Steel	100	492.5	0.125 ¹	8.71	0.587 for DSC shell, 0.35 for heat shields
	150			9.00	
	200			9.29	
	250			9.58	
	300			9.79	
	350			10.08	
	400			10.37	
	450			10.58	
	500			10.87	
	550			11.09	
	600			11.30	
800	12.17				

Table Notes: 1) A fixed specific heat value used for simplicity since calculation is for steady-state conditions.

Table 3-2 - Material Properties, Air

Temperature °F	Density lbm/in ³	Specific Heat Btu/lbm-°F	Conductivity Btu/hr-ft-°F	Viscosity lbm/ft-sec
80	4.20E-05	0.2404	0.0151	1.2447E-05
260	3.15E-05	0.2427	0.0191	1.5406E-05
440	2.52E-05	0.2464	0.0228	1.8019E-05

A TRANSNUCLEAR

PROJECT NO: SCE-23	REVISION: 2
CALCULATION NO: SCE-23.0410	PAGE: 10 of 65

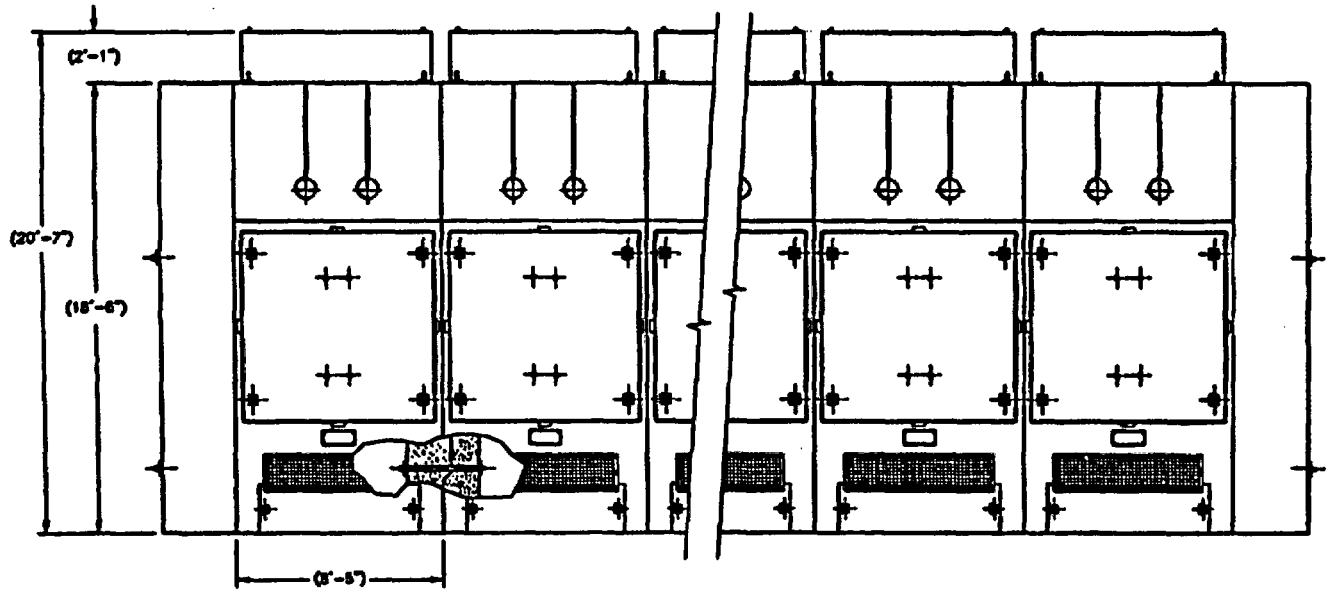


Figure 3-1 - Illustration of Typical NUHOMS AHSM Storage Array

A TRANSNUCLEAR

PROJECT NO: SCE-23	REVISION: 2
CALCULATION NO: SCE-23.0410	PAGE: 11 of 65

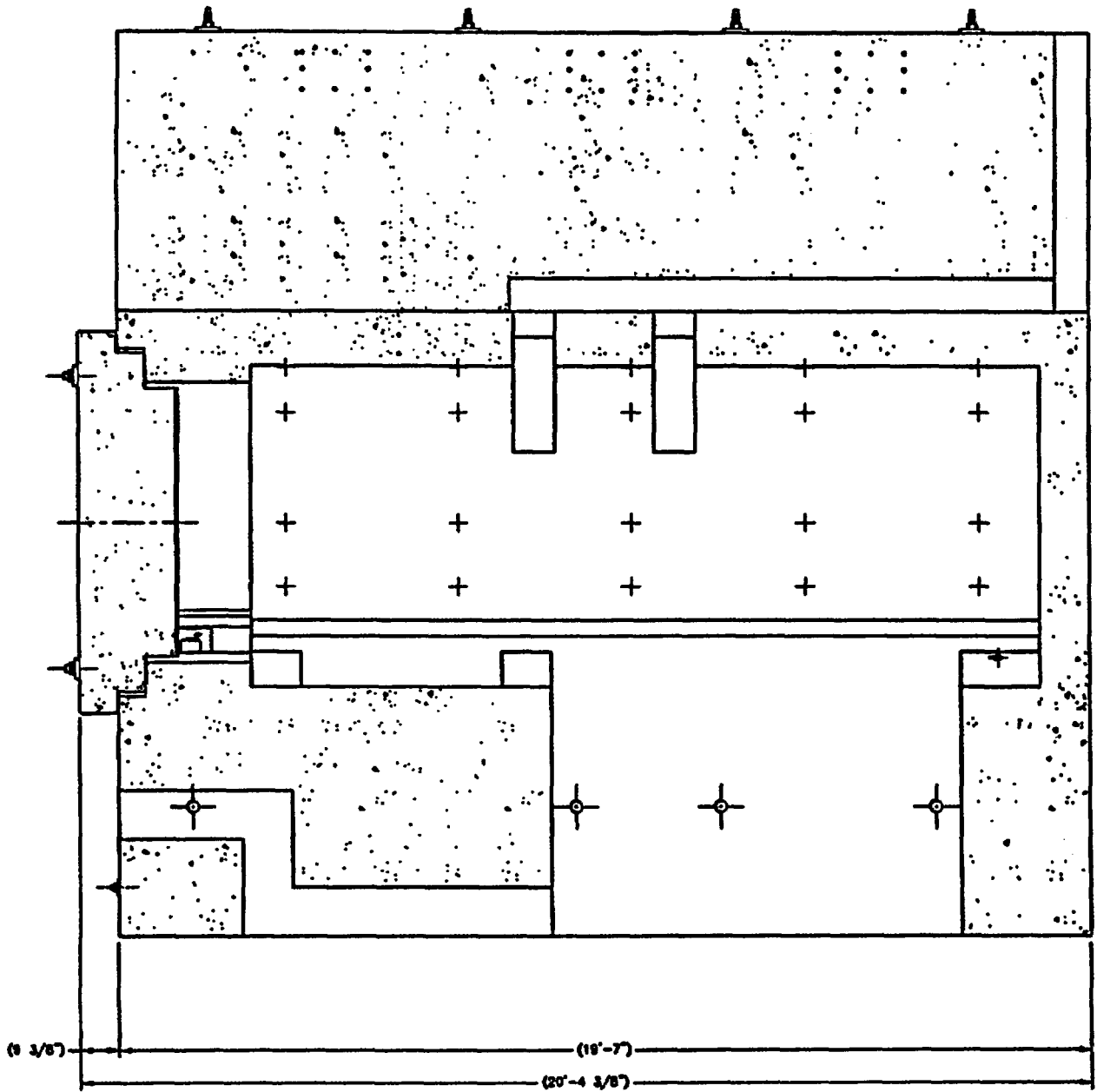


Figure 3-2 - Cross-Section View Through Center Of AHSM Module

A

TRANSNUCLEAR

PROJECT NO: SCE-23	REVISION: 2
CALCULATION NO: SCE-23.0410	PAGE: 12 of 65

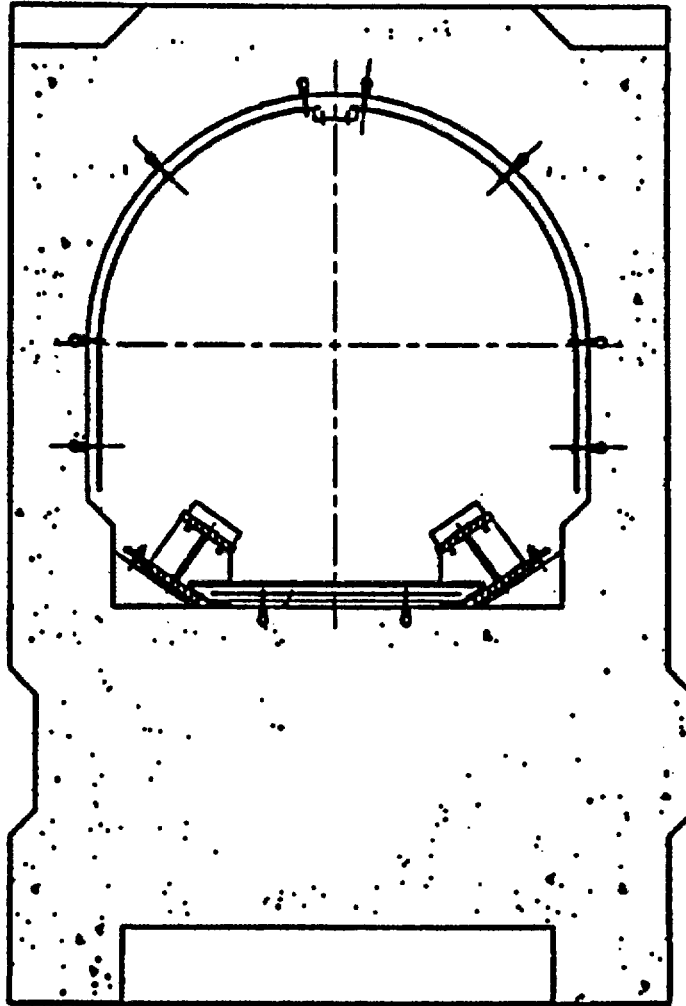


Figure 3-3 - View Of DSC Support Structure & Heat Shields

PROJECT NO: SCE-23	REVISION: 2
CALCULATION NO: SCE-23.0410	PAGE: 13 of 65

4. CALCULATIONS

4.1 Fluent™/ Icepak™ Model

Based on the AHSM geometry summarized in Section 3.1 and detailed in the [6.2] drawing set, the thermal-hydraulic environment within the AHSM storage module is evaluated for the bounding hot and cold day conditions and a DSC decay heat loading of 24 kW. The program selected for this evaluation is the Fluent™ code [6.5] with the Icepak™ module [6.6]. The Fluent™ code is a general purpose computational fluid dynamics (CFD) code that is recognized internationally as one of the premier codes in its class. The general modeling capabilities of the code as they relate to this application include:

- Meshing flexibility using structured and unstructured mesh generation with hexahedra, non-hexahedra, and tetrahedral mesh types
- Capability to model low speed, buoyancy driven flow regimes
- Steady-state and transient flows
- Inviscid, laminar, and turbulent flows
- Heat transfer including forced, natural, and mixed convection, conjugate heat transfer, and radiation
- Custom materials property database
- Integrated problem set-up and post-processing

The Icepak™ module is a fully interactive, object-based graphical interface that allows complex geometries to be modeled and meshed using a combination of shapes in a 'building block' approach. The Icepak™ module does not perform any CFD related numerical calculations itself, but only serves as a pre- and post-processor to the Fluent™ code. While the Icepak™ module is specifically designed for the analysis of electronic enclosures, its operational features are fully capable of handling the geometry for this application.

The verification and validation of the Icepak™ and Fluent™ codes for the computation of generic buoyancy driven convection heat transfer within an enclosure is documented in [6.7]. Further validation of the codes for handling the convection and radiation heat transfer specific to a horizontal storage module is provided in [6.7], wherein the codes are used to simulate the full scale test results for a NUHOMS® 7P canister in a horizontal storage module [6.8]. That testing evaluated the thermal performance of the NUHOMS® 7P DSC using a combination of electrical heaters and actual spent fuel assemblies. The validation analysis showed that application of the same CFD modeling approach as used in this calculation to the modeling of the NUHOMS® 7P canister in a horizontal storage module yielded conservatively high temperature predictions for the DSC shell and the heat shields, while matching within 3 °F the measured peak concrete temperature.

Figure 4-1 illustrates an isometric wire frame view of the thermal-hydraulic model developed for this evaluation. The +x axis of the model's coordinate system extends across the 101" width of the module from left to right when facing the front of the module. The +y axis is aligned with the

A TRANSNUCLEAR

PROJECT NO: SCE-23	REVISION: 2
CALCULATION NO: SCE-23.0410	PAGE: 14 of 65

elevation of the module with the 0 dimension at the top of the base mat and the maximum 222" dimension at the top of the module's roof. The +z axis extends 235" from the back of the module to the front face of the module.

As seen from the partial solid shaded depiction in Figure 4-2, the model accurately captures the geometry of the curved vault structure of the AHSM along the two vertical air ducts leading from the vault to the horizontal exhaust duct in the roof of the AHSM. While a symmetry plane can be assumed along a y-z plane through the center of the module, a full 3-D model is used since radiative exchange is a major heat transfer mode within the AHSM module and a symmetry model would not permit the correct calculation of the view or shape factors.

The concrete walls and roof of the module are modeled using a combination of block shapes. Figure 4-2 and Figure 4-3 illustrate portions of the modeled geometry of the side, base, and back walls of the module. The program automatically handles the thermal connections between the various model blocks to create a unified thermal model of the concrete sections. As illustrated in Figure 4-3, the geometry of the angled support rails and concrete support blocks are accurately captured by the thermal model.

Figure 4-4 illustrates the geometry of the modeled inlet duct within the base unit. The dimensions and sharp 90° turns of the modeled duct match the actual flow path within the AHSM. A screened opening with a loss coefficient of 0.58 is assumed at the front of the module.

The modeling of the DSC within the AHSM module (see Figure 4-5) is accomplished using polygon blocks to form a twenty-four (24) sided representation of the DSC. This representation is used for the cylindrical DSC (i.e., 196.3" long x 67.19" diameter) since the surface-to-surface radiation methodology implemented within the IcePak module applies the computed view factors across the entire surface instead of over a sub-set of the surface mesh. As such, to prevent 'smearing' computed view factors around the cylindrical shape of the DSC, 24 polygon shapes are used to break the DSC into individual surfaces. Since the number of segments used closely approximates the circular cross section of the DSC, the modeling approach has a minor impact on the flow regime around the DSC and provides a conservative representation of the DSC's surface area.

A 6.88-inch long solid block is used to represent the bottom shield plug and a 8.75-inch long solid block is used to represent the top shield plug. These dimensions represent slight increased lengths from the minimum dimensions specified in general assumption #2.1.4 with the increased dimensions made to improve the computational mesh generated for the model. The 180.67-inch long (i.e., 196.3" maximum DSC length - 6.88" - 8.75"), 0.5-inch thick shell of the DSC is simulated by dividing the DSC shell into 5 axial segments with lengths of 4", 50", 50", 50", and 26.67" from bottom to top, respectively. At each axial segment, twenty-four (24) 0.5-inch thick polygon blocks, each spanning 15° of the circumference of the DSC, are used to approximate the cylindrical shape of the DSC shell. Based on the support structure design and assuming the DSC is pushed all the way back until it mates with the canister stops, the top of the DSC begins 7.25-inches from the back wall of the module.

A TRANSNUCLEAR

PROJECT NO: SCE-23	REVISION: 2
CALCULATION NO: SCE-23.0410	PAGE: 15 of 65

The fuel basket is not specifically modeled. Instead, the decay heat loading is simulated as a uniform heat flux applied over the 150", corresponding to the active fuel length of the CE 16x16 FAs. Allowing for the bottom nozzle height of the FA, the active fuel region is assumed to begin 4" above the bottom shield plug.

Figure 4-6 illustrates the model geometry for the heat shields within the AHSM. As seen, the curved shape of the upper heat shields is captured, as is the placement of the inner heat shield at the top of the AHSM's vault. The heat shields are modeled using thin conducting plate elements.

The final flow turn before the outlet opening and the wire mesh at the screened opening is not specifically modeled in order to simplify the modeling and since the flow losses associated with these flow path items have been well defined by experimental testing [6.4]. Instead, a combined flow loss factor, based on the approach velocity, is applied as a flow resistance element at the outlet. The loss factors are 0.58 for the screened opening, plus 1.0 for the diverging tee turn, or a total flow loss coefficient of approximately 1.6.

The ability of the Fluent™ program to create non-conformal computational meshes is utilized to concentrate the mesh density areas requiring greater fluid flow and/or thermal resolution and decrease the mesh density in areas (i.e., within the concrete walls, etc.) that do not experience large thermal gradients. The use of non-conformal meshes greatly reduces the size of the problem to be solved, while not negatively impacting the accuracy of the solution. The resultant non-conformal mesh used for this evaluation is illustrated in Figure 4-7 to Figure 4-9. A total of approximately 1,260,300 mesh elements are used for the analysis. Figure 4-7 presents a perspective view of the mesh profile along the x-y plane through the center of the module. The concentration of the mesh in the vicinity of the DSC and in the outlet duct within the concrete roof is clearly evident from the figure.

Figure 4-8 presents an enlarged view of the mesh in the vicinity of the DSC support structure. The mesh across the thickness of the DSC shell within the support rails, and at the angled surface of the concrete support blocks is evident. Further, the difference in mesh density between the computational regions can be seen. The boundaries between the computational regions lie within the concrete structure. The program uses an interpolation routine to transfer solution data from one mesh region to the other during the solution procedure.

Figure 4-9 illustrates an elevation view of the mesh profile along the y-z plane through the center of the module. The non-conformal nature of the mesh is again evident from the figure with the mesh density being significantly higher in the region of the inlet duct, the DSC shell and heat shields, and the outlet duct and much lower elsewhere.

The CFD analysis is conducted with radiation and turbulent flow enabled. The radiation view factors were calculated using the 'hemicube' methodology, with the mesh coarsening option disabled to avoid lessening the resolution for the curved and angled surface shapes. The effects of flow turbulence are calculated using the 'mixing-length zero-equation' turbulence model, while the temperature-dependent fluid density is computed using the Boussinesq model. Both of these computational options represent the FLUENT recommendations for natural convection, buoyancy



TRANSNUCLEAR

PROJECT NO: SCE-23	REVISION: 2
CALCULATION NO: SCE-23.0410	PAGE: 16 of 65

driven problems. The appropriateness of assuming a turbulent flow regime was validated via a sensitivity run wherein only a laminar flow regime was permitted and another sensitivity run using the 2-equation turbulence model with wall enhancements. Both sensitivity runs produced results that were similar to those obtained with 'mixing-length zero-equation' turbulence model. The use of the Boussinesq model was also validated via a sensitivity run wherein the use of the ideal gas option to compute density produced similar peak temperatures.

Direct simulation of insolation on the outer surface of the AHSM could not be included in the selected modeling approach due to program limitations on the number of boundary conditions that can be applied at each surface. Therefore, the simulation of the insolation was addressed by increasing the reference temperature used to compute the convective and radiation heat transfer exchange from the affected surfaces to account for the insolation heating of the surface. The effect of insolation heating on the horizontal roof surface for the normal hot storage condition can be estimated by computing the surface temperature required to dissipate the incident insolation back into the ambient environment. For regulatory conditions, the 24-hour averaged insolation on a flat, horizontal surface is 122.7 Btu/hr-ft². To dissipate this heat load, a surface would have to be at a temperature of 155.6°F (i.e., an increase of 58.6°F from the average 97°F ambient temperature assumed for the normal hot storage condition). At this temperature, the heat loss into a 97°F environment from a horizontal surface via convection and radiation would be: $0.85 \text{ Btu/hr-ft}^2\text{-}^\circ\text{F} \times (155.6^\circ\text{F} - 97^\circ\text{F}) + 1.712 \times 10^{-9} \times 0.9 \times [(459.67 + 155.6^\circ\text{F})^4 - (459.67 + 97^\circ\text{F})^4] = 122.7 \text{ Btu/hr-ft}^2$, where 0.85 Btu/hr-ft²-°F is a representative convection coefficient for a heated surface facing upward and 0.9 is the emissivity of unpainted concrete.

Similarly, the 24-hour averaged insolation on a flat, vertical surface is 30.7 Btu/hr-ft². To dissipate this heat load, a surface would have to be at a temperature of 114.5°F (i.e., an increase of 17.5°F from the average 97°F ambient temperature assumed for the normal hot storage condition). At this temperature, the heat loss into a 97°F environment from a vertical surface via convection and radiation would be $0.65 \text{ Btu/hr-ft}^2\text{-}^\circ\text{F} \times (114.5^\circ\text{F} - 97^\circ\text{F}) + 1.712 \times 10^{-9} \times 0.9 \times [(459.67 + 114.5^\circ\text{F})^4 - (459.67 + 97^\circ\text{F})^4] = 30.9 \text{ Btu/hr-ft}^2$, where 0.65 Btu/hr-ft²-°F is a representative convection coefficient for a vertical surface and 0.9 is the emissivity of unpainted concrete.

Zero insolation is assumed for the off-normal cold storage condition. Adiabatic conditions are assumed for the side and back walls of the module.

4.2 Thermal Analysis at Bounding Design Basis Ambient Condition

Figure 4-10 to Figure 4-17 present a summary of the surface temperature distributions predicted for the analyzed decay heat loading of 24 kW within the DSC, the bounding normal hot day condition with a peak daily temperature of 104°F and a 24-hour average of 97°F, and the insolation. Figure 4-10 to Figure 4-12 illustrates the predicted temperature profile on the DSC surface. The temperature variation over the surface of the DSC reflects the combination of the heat flux applied to the shell, the difference in view factors between the DSC surface and the various components of the AHSM, and the distribution airflow within the AHSM as influenced by the presence of the support structure and the location of the outlet ducts. As seen from the figures, the maximum surface temperature predicted is 459°F. Further, this analysis predicts a maximum temperature of 397°F at the side of the

A TRANSCLEAR

PROJECT NO: SCE-23	REVISION: 2
CALCULATION NO: SCE-23.0410	PAGE: 17 of 65

DSC (see Figure 4-11) and 367°F at the bottom of the DSC (see Figure 4-12). In comparison, the [6.1] analysis predicts DSC shell temperatures of 399°F and 351°F at the top and bottom of the DSC shell, respectively.

As such, the principal difference in the predicted DSC shell temperatures between this calculation and the [6.1] results is the higher temperature along the top of the DSC predicted by the CFD analysis. While the top of a horizontal cylinder in a natural, buoyancy-driven flow field is the classic region for elevated temperature to develop, the extent of the region of elevated temperatures and the magnitude of the temperature rise are amplified by the close proximity of the inner heat shield which prevents the airflow from rising directly upwards. Instead, as the CFD analysis demonstrates (see Figure 4-24), the flow is restricted and is required to turn back on itself in order to exit from underneath the inner shield. Both effects, not accounted for in the [6.1] analysis, lead to the elevated temperature seen in the CFD analysis. Due to the blocking effect of the support rails on the airflow, the CFD analysis predicts a hotter temperature at the bottom of the DSC shell vs. its side outside of the rails (i.e., 367°F vs. 357°F). In contrast, the [6.1] analysis, ignored the presence of the support rail and predicts a nearly uniform increase in the shell temperature around the DSC from the bottom to the top. The conduction into the support rails from the DSC is evident in Figure 4-12 by the twin 'lines' of cooler temperature on the surface of the DSC.

Figure 4-13 illustrates the temperature profile on the heat shields within the AHSM module. A maximum temperature of 314°F occurs on the inner heat shield at the top of the vault. A peak temperature of 276°F occurs on the upper heat shield at the top of the vault. In comparison, the [6.1] analysis predicts a peak heat shield temperature of 258°F. The elevation view of the temperature distribution in the heat shield illustrated in Figure 4-14 shows the expected results of higher temperatures with increased elevation. The variation in temperature from back to front on the heat shield reflects the computed distribution of airflow over the DSC.

Figure 4-15 depicts the temperature distribution over a portion of the concrete walls of the base unit, while Figure 4-16 illustrates the temperature distribution over the vault portion of the module. The analysis predicts a peak concrete temperature of 212°F at the back wall and 232°F at the inside surface of the vault. The [6.1] analysis predicts a peak temperature of 219°F for these same locations. The maximum temperature of 281°F for the DSC support structure occurs at the point of contact between the rails and the DSC temperature. Since the [6.1] analysis did not specifically model the support structure components, it conservatively assumed its peak temperature along the bottom of the DSC of 351°F for the maximum support rail temperature.

Figure 4-17 presents an elevation view of the predicted temperature distribution along an axial plane through the module. The figure reflects the expected temperature distribution given the general airflow paths and the presence of the DSC. Figure 4-18 presents the temperature variation at the exhaust outlet and Figure 4-19 illustrates the variation in the flow velocity at the same location. The peak temperature at the exhaust vent is 212°F, while the average exhaust air temperature is 196°F. As such, the predicted air temperature rise through the AHSM is $196 - 97 = 99^\circ\text{F}$ vs. the 96.4°F predicted by the [6.1] analysis. The predicted airflow rate is 0.85 lbm/sec. The analysis indicates that 21.4 kW of the 24 kW decay heat loading (i.e., 89%) is removed via the air stream. Inclusion of the extra 8



TRANSNUCLEAR

PROJECT NO: SCE-23	REVISION: 2
CALCULATION NO: SCE-23.0410	PAGE: 18 of 65

inches of mean stack height represented by the exit vent roof cap which was not modeled could lower the computed 99°F air temperature rise through the AHSM by another 2 to 3°F, based on the square root of the change in the effective chimney height.

Figure 4-20 to Figure 4-27 present the flow velocity profiles at selected locations within the AHSM module. Note that the velocity scale in each figure is re-scaled to span the range of velocities occurring within the depicted view. Figure 4-20 illustrates the profiles along an x-y plane through the middle of the second (i.e., rear) vertical flow duct out of the AHSM vault. The profile shows the expected trend of low flow velocity with regions of re-circulation within the lower plenum and between the support rails, increasing flow velocity around the DSC due to the smaller flow space and as the air is heated and expands, and the maximum velocity achieved at exit flow ducts. A similar flow distribution is noted in Figure 4-21 which depicts the profile along a x-y plane through the middle of the AHSM and Figure 4-22 which illustrates the predicted flow profile at an x-y plane through the middle of the first (i.e., front) vertical flow duct.

Figure 4-23 presents an enlargement of Figure 4-22 in the vicinity of the support structure. While the blocking effect of the support rails can clearly be seen in the figure, it is also evident that no 'dead air' region occurs between the rails. Figure 4-24 presents an enlargement of Figure 4-22 in the vicinity of the top of the AHSM vault and the DSC. The figure illustrates a uniform flow over the exterior of the DSC, with a zone of flow separation at the top of the DSC. This 'low flow' zone leads to the region of elevated temperatures noted on the DSC temperature distribution depicted in Figure 4-10.

Figure 4-25 illustrates the flow profile along a y-z plane through the center of the module. The figure depicts the expected regions of flow recirculation within the inlet duct and plenum below the DSC. The figure also shows that, despite interior obstructions, the airflow is relatively evenly distributed along the length of the DSC. A maximum flow velocity of approximately 5.6 feet per second is seen to occur in the vertical exhaust duct at the rear of the module. This peak velocity is conservative since, as explained in Section 2.2, the vertical exhaust channel is modeled 16" narrower than the actual dimension. As such, the actual peak flow velocity will be approximately 20% less or 4.5 ft/sec.

Figure 4-26 presents an enlargement of Figure 4-25 in the vicinity of the vault roof ducts. The flow profile depicts the expected flow contraction as the air enters the sharp edge outlet ducts, the region of flow recirculation at the corner of the roof duct (see the left side of the figure), and the disturbance on the airflow from the front vault duct as the airflow from the rear vault duct enters the roof duct.

Figure 4-27 presents the profile along a y-z plane approximately 24 inches from the edge of the module. Again, the figure demonstrates that the module's airflow will be relatively evenly distributed along the length of the vault. Figure 4-27 presents an enlargement of Figure 4-25 in the vicinity of the inlet duct. The flow profile shows the expected effect of the double, sharp angle turns in that regions of flow recirculation develop at the corners of the turns and the fact that the flow velocities are highly skewed across the width of the duct. These effects are in line with the

A TRANSNUCLEAR

PROJECT NO: SCE-23
CALCULATION NO: SCE-23.0410

REVISION: 2
PAGE: 19 of 65

empirically predicted flow losses that references, such as [6.4], show for duct arrangements of this type.

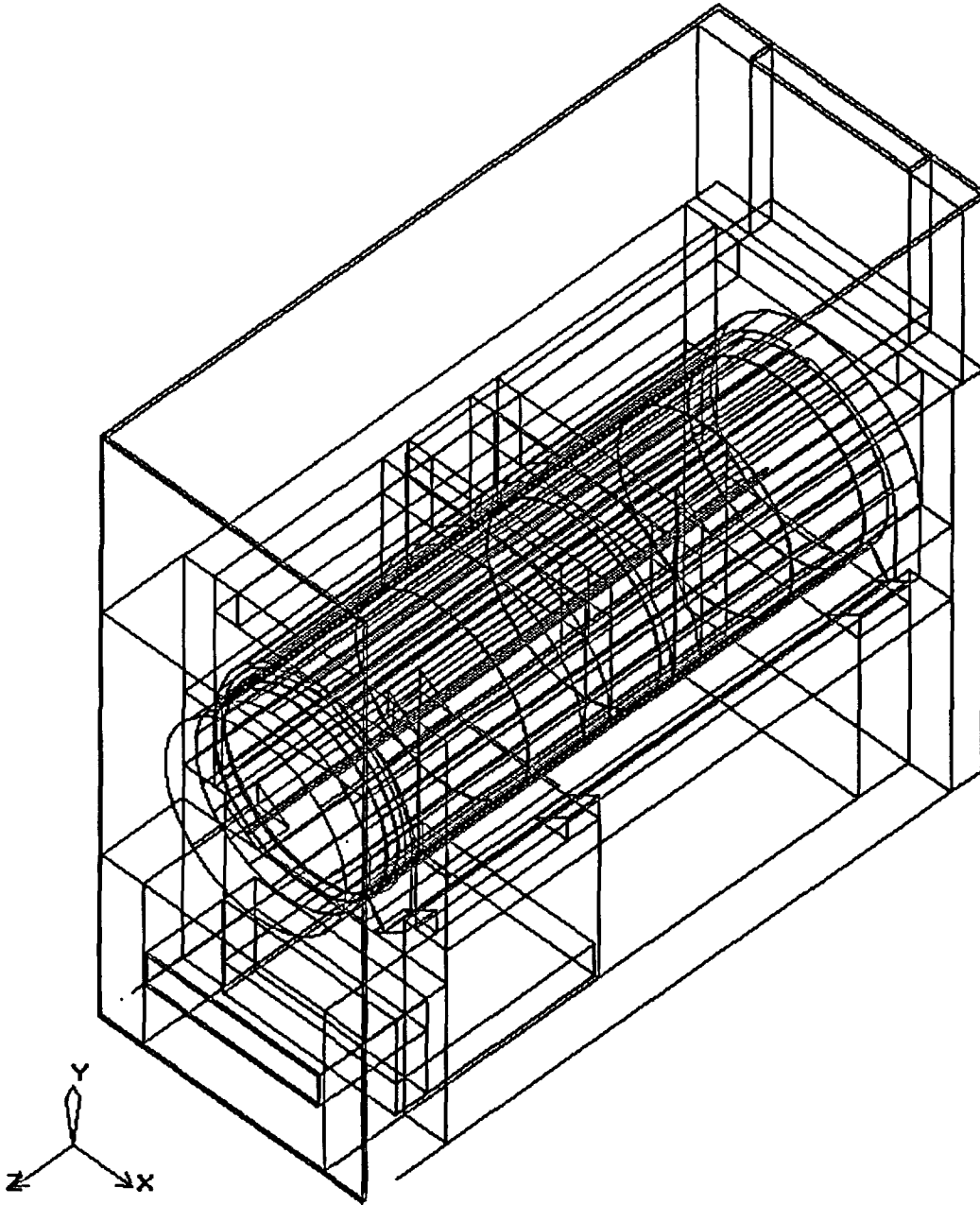


Figure 4-1 - Isometric, Wireframe View Of Model Layout

A

TRANSNUCLEAR

PROJECT NO: SCE-23	REVISION: 2
CALCULATION NO: SCE-23.0410	PAGE: 20 of 65

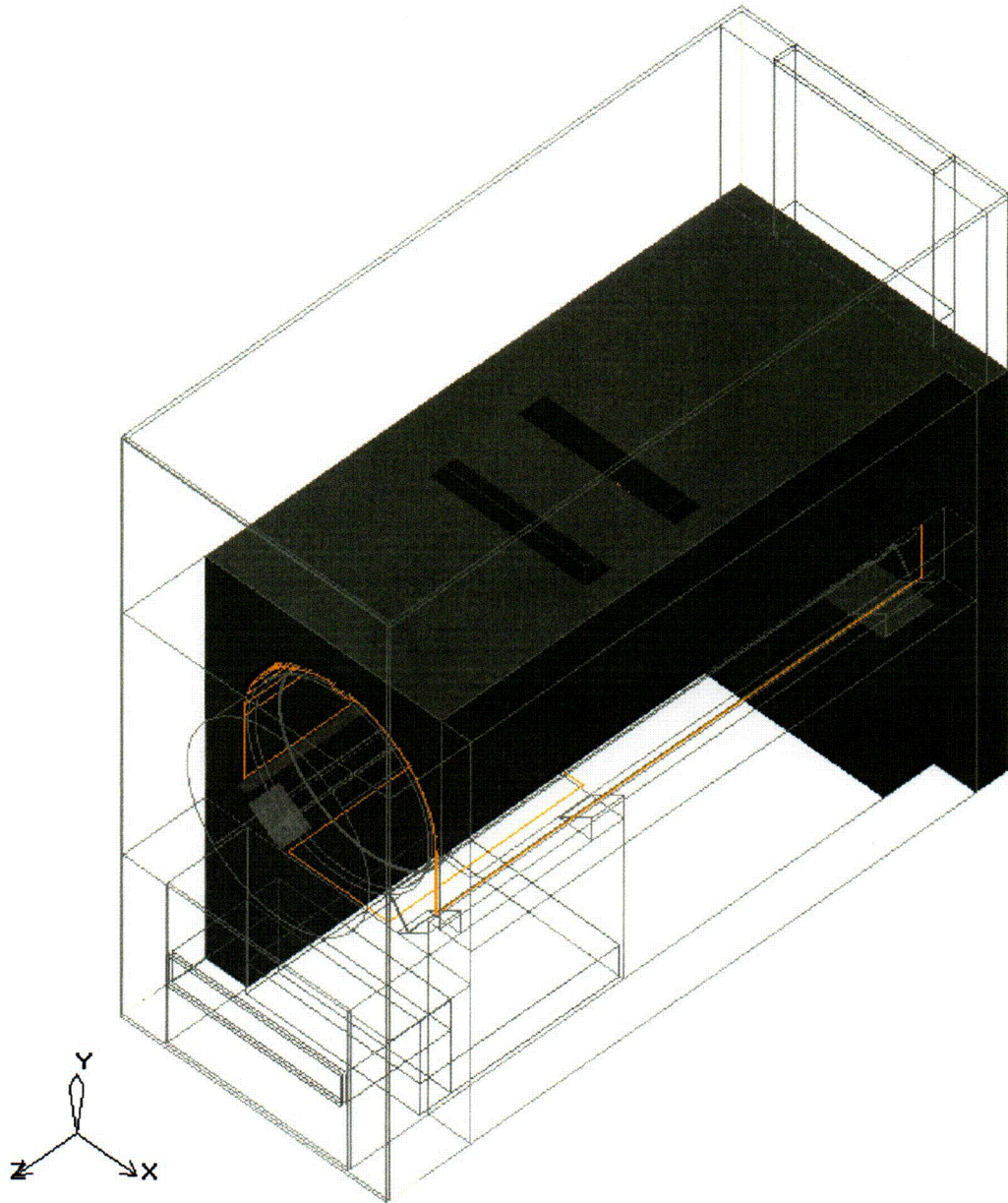


Figure 4-2 - Cutaway View #1 Of Module Base Unit Model

C01

A TRANSNUCLEAR

PROJECT NO: SCE-23	REVISION: 2
CALCULATION NO: SCE-23.0410	PAGE: 21 of 65

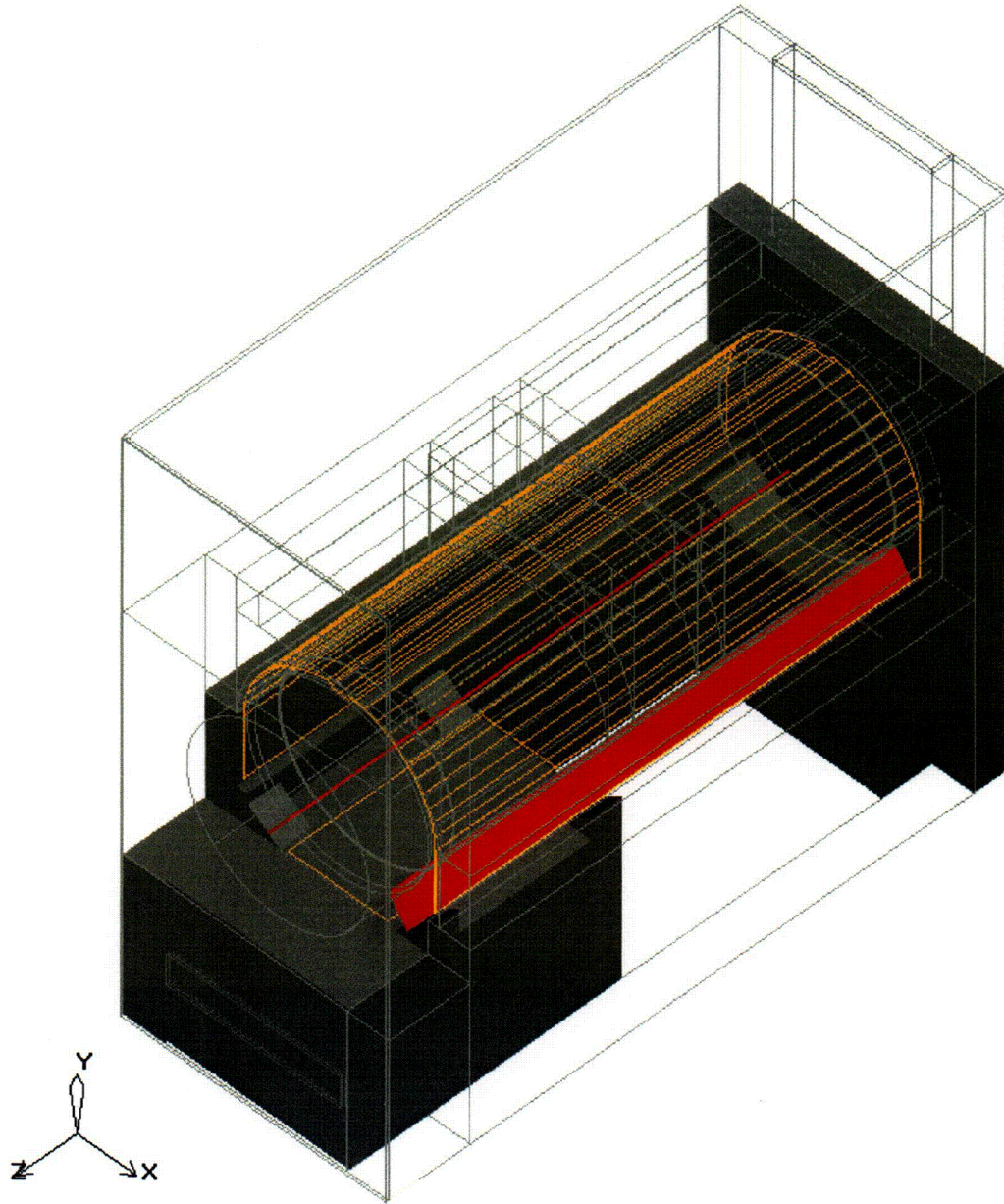


Figure 4-3 - Cutaway View #2 Of Module Base Unit Model

CO2

A TRANSNUCLEAR

PROJECT NO:	SCE-23	REVISION:	2
CALCULATION NO:	SCE-23.0410	PAGE:	22 of 65

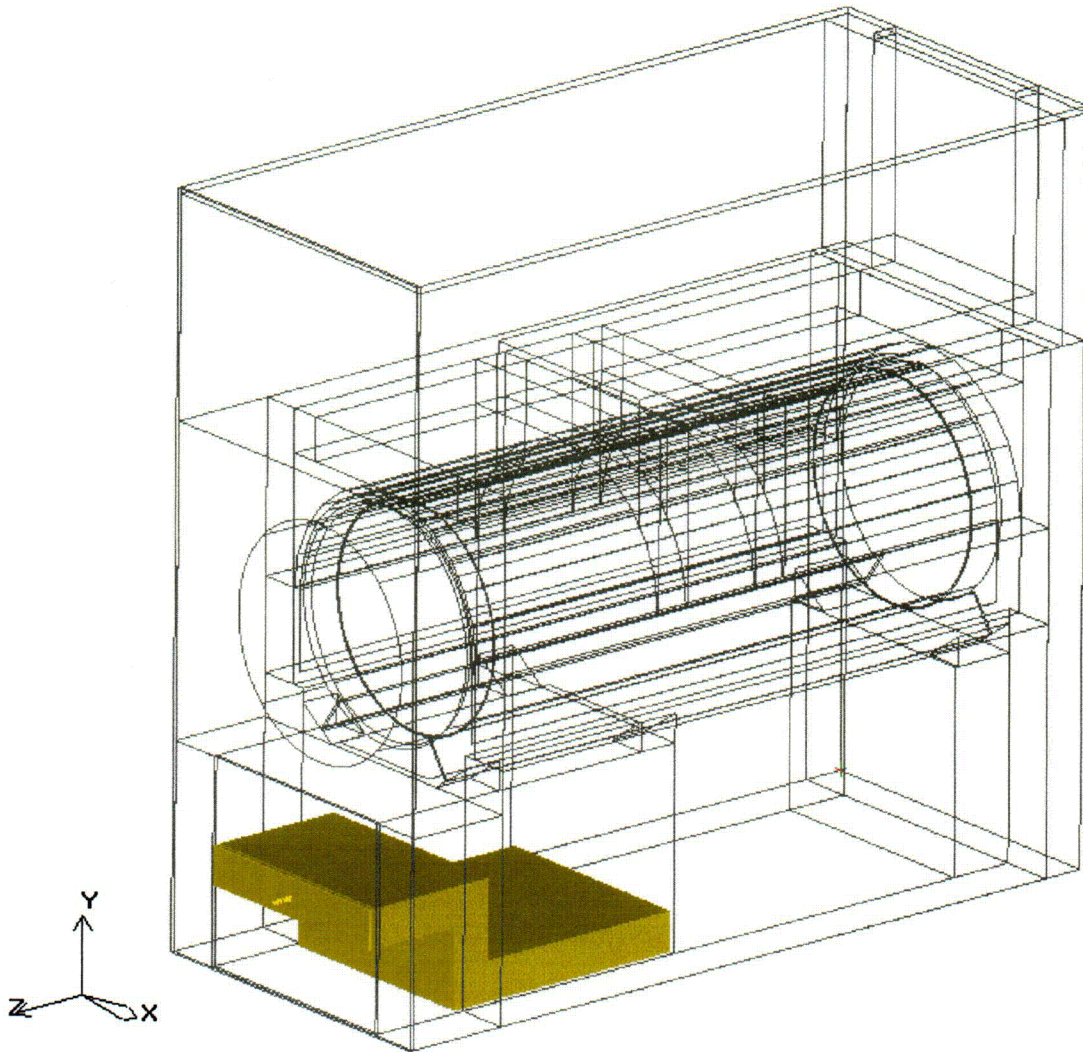


Figure 4-4 - View Of Inlet Duct For Module Base

C03

A TRANSNUCLEAR

PROJECT NO: SCE-23
CALCULATION NO: SCE-23.0410

REVISION: 2
PAGE: 23 of 65

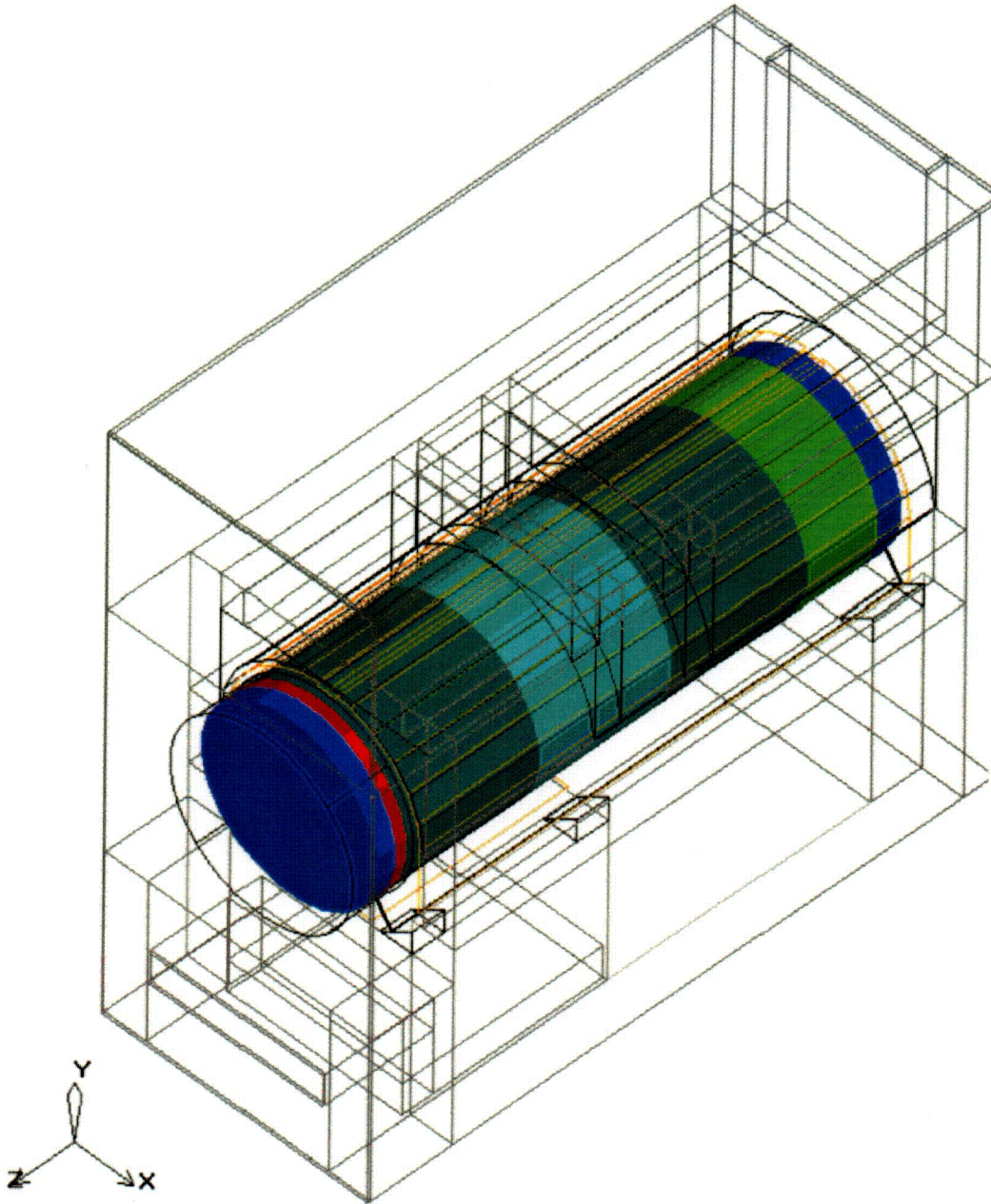


Figure 4-5 - Isometric View Of Seven (7) Segments Used To Simulate DSC Within Module

A TRANSNUCLEAR

PROJECT NO: SCE-23

CALCULATION NO: SCE-23.0410

REVISION: 2

PAGE: 24 of 65

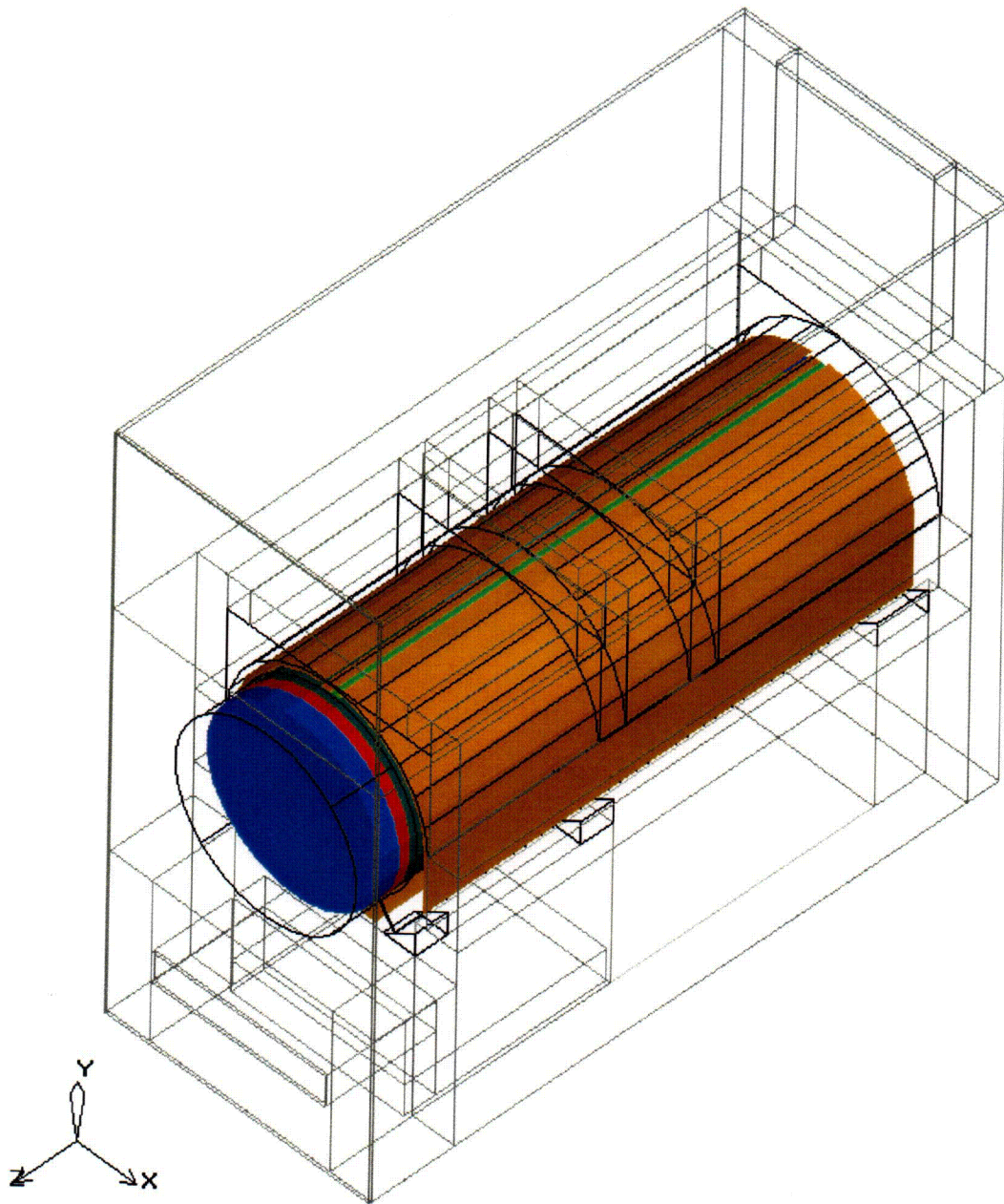


Figure 4-6 - Isometric View Of DSC & Heat Shield Layout Within Model

C05

B-2-cal-00

A TRANSNUCLEAR

PROJECT NO: SCE-23
CALCULATION NO: SCE-23.0410

REVISION: 2
PAGE: 25 of 65

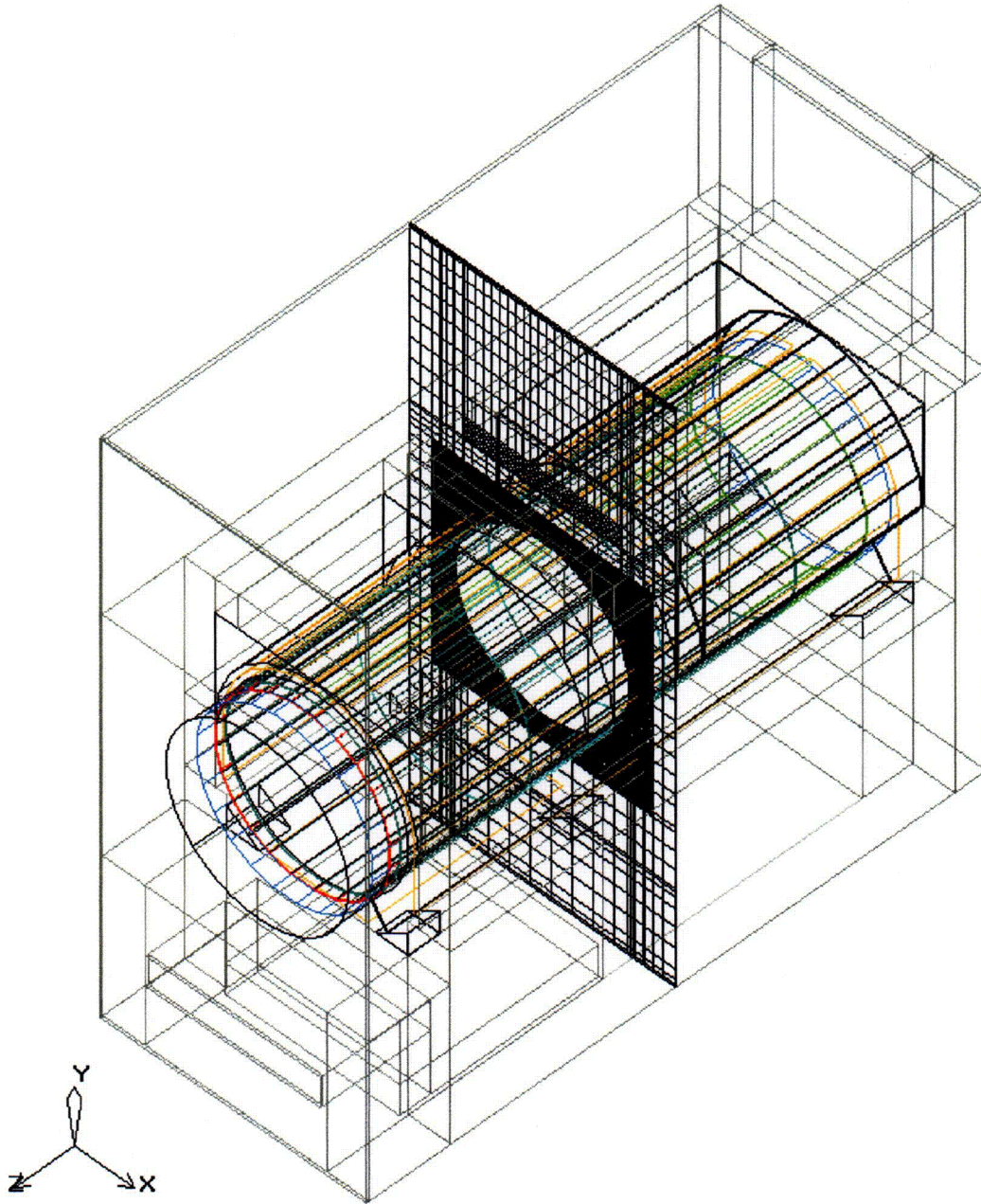


Figure 4-7 - Perspective View Of Meshing At X-Y Plane Of AHSM

C06

A

TRANSNUCLEAR

PROJECT NO: SCE-23	REVISION: 2
CALCULATION NO: SCE-23.0410	PAGE: 26 of 65

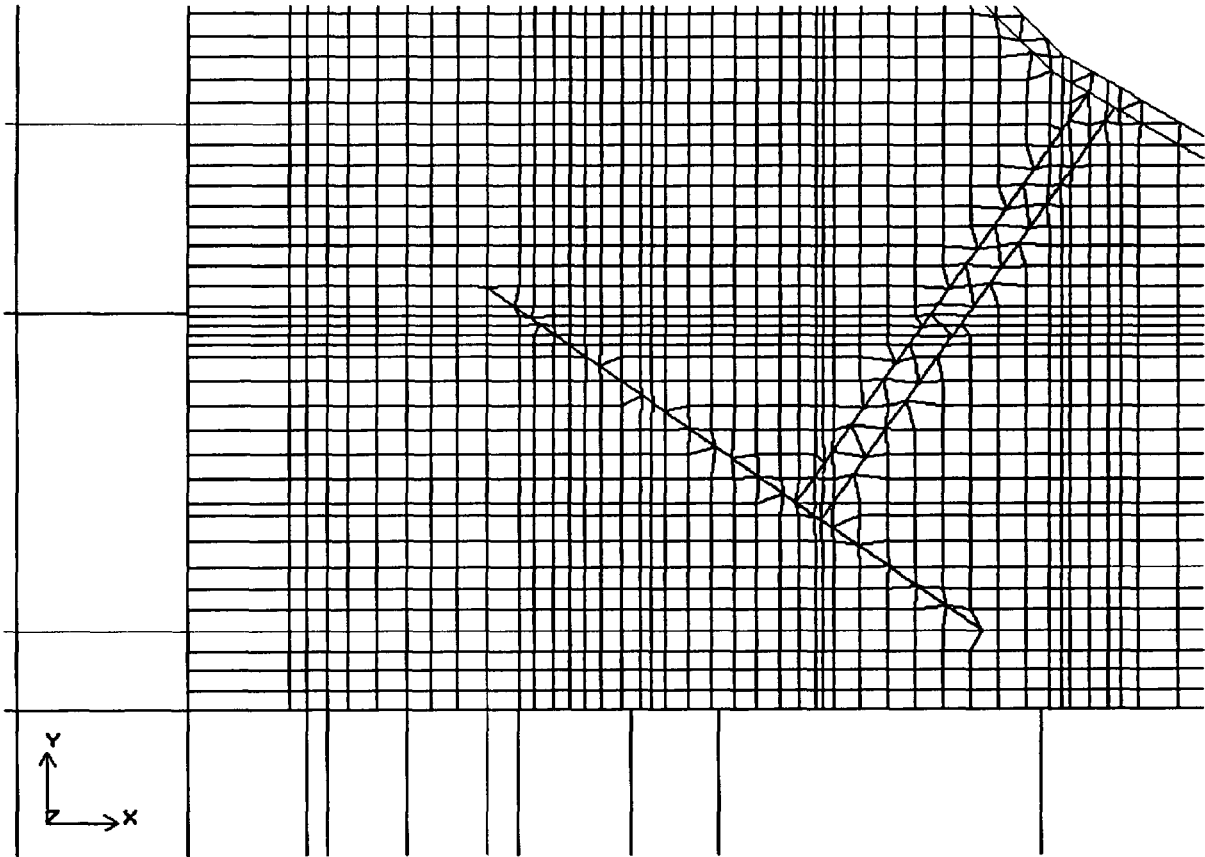


Figure 4-8 - Enlarged View Of Meshing At DSC Support Structure

A TRANSNUCLEAR

PROJECT NO:	SCE-23	REVISION:	2
CALCULATION NO:	SCE-23.0410	PAGE:	27 of 65

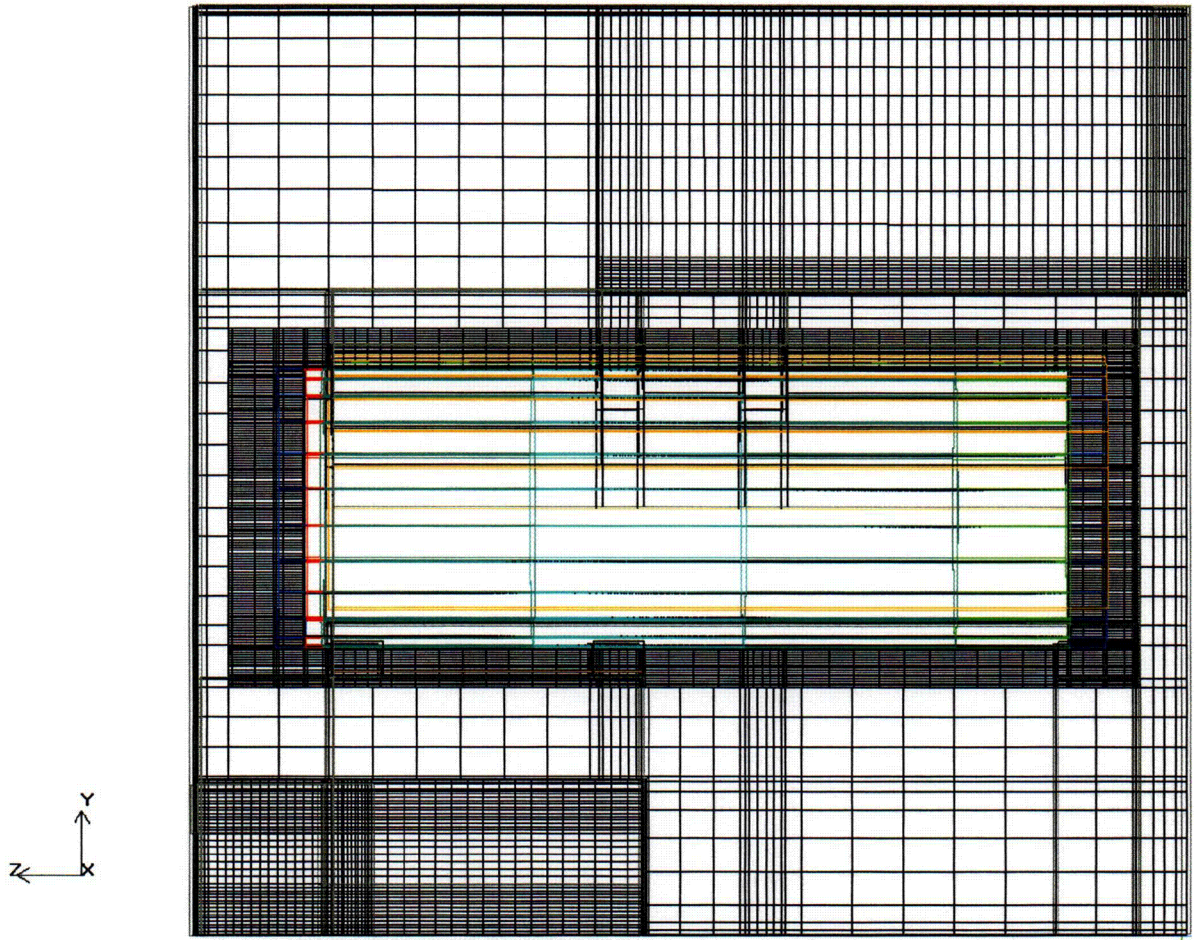


Figure 4-9 - Elevation View Of Meshing At Z-Y Plane Of AHSM

C07

A TRANSNUCLEAR

PROJECT NO: SCE-23	REVISION: 2
CALCULATION NO: SCE-23.0410	PAGE: 28 of 65

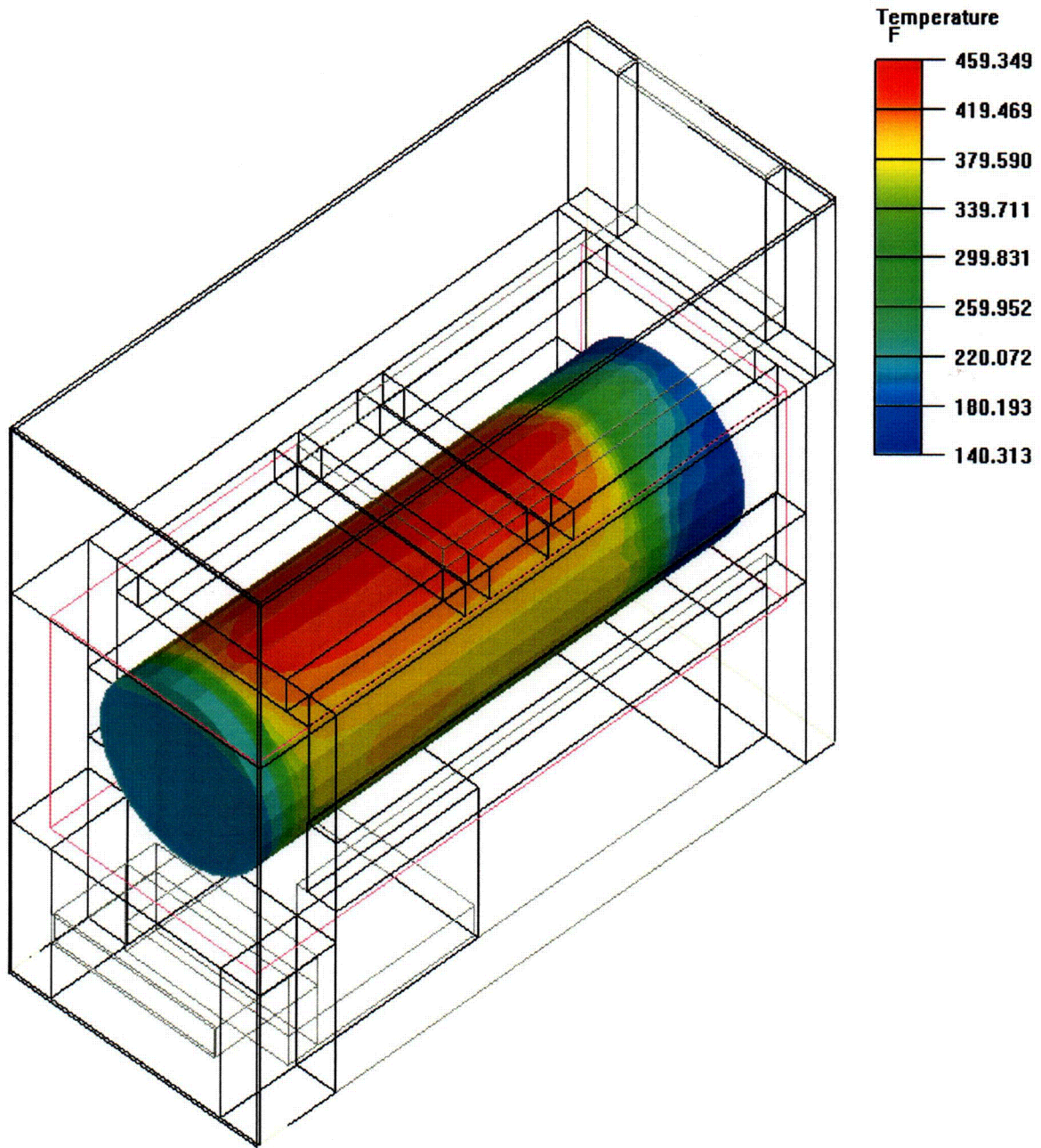


Figure 4-10 - Temperature Distribution On DSC Surface, Perspective View, Normal Hot Storage Condition

C08

PROJECT NO: SCE-23	REVISION: 2
CALCULATION NO: SCE-23.0410	PAGE: 29 of 65

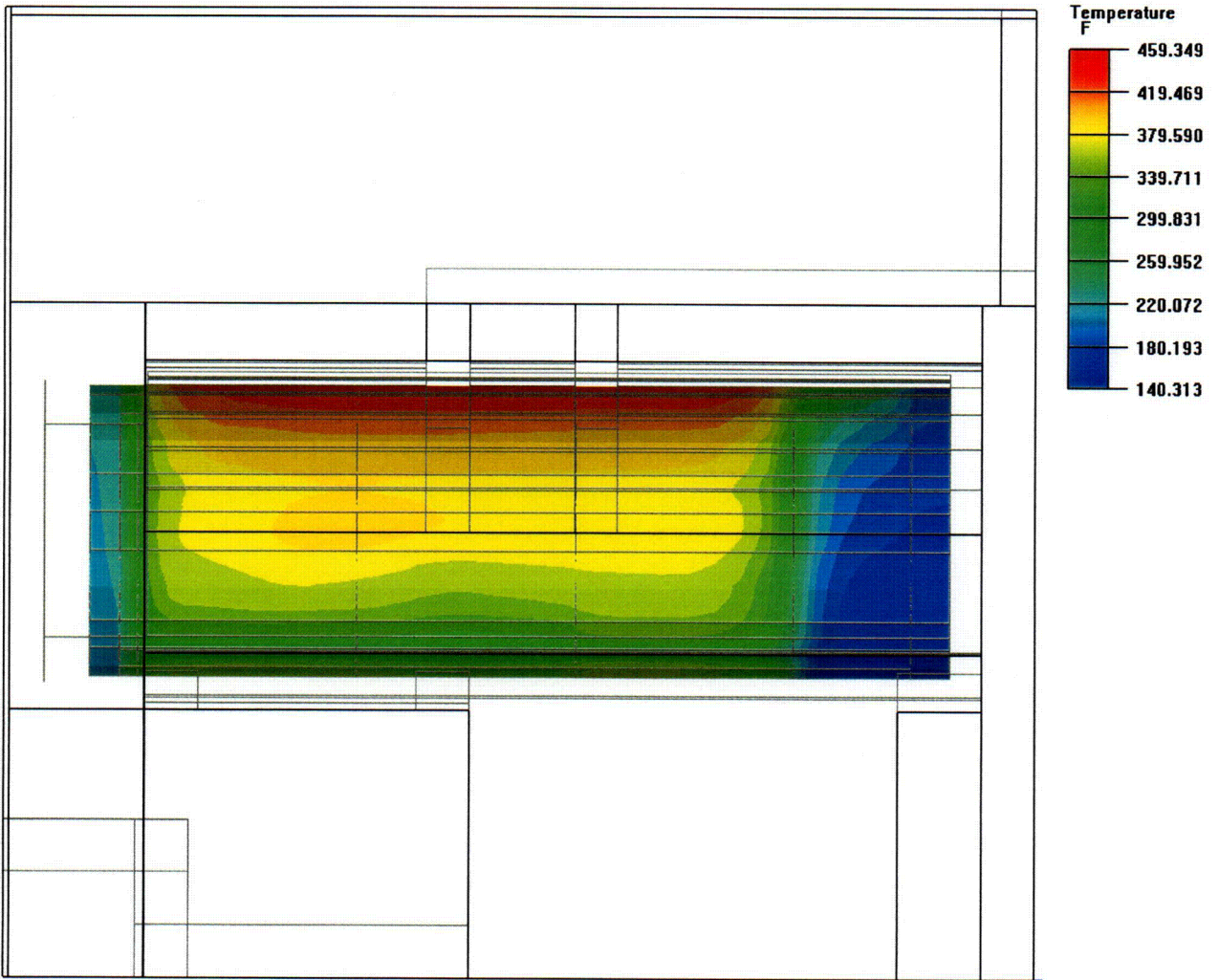


Figure 4-11 - Temperature Distribution On DSC, Side View, Normal Hot Storage Condition

(Note: Front face of AHSM module is at left side of figure)

C09

PROJECT NO: SCE-23	REVISION: 2
CALCULATION NO: SCE-23.0410	PAGE: 30 of 65

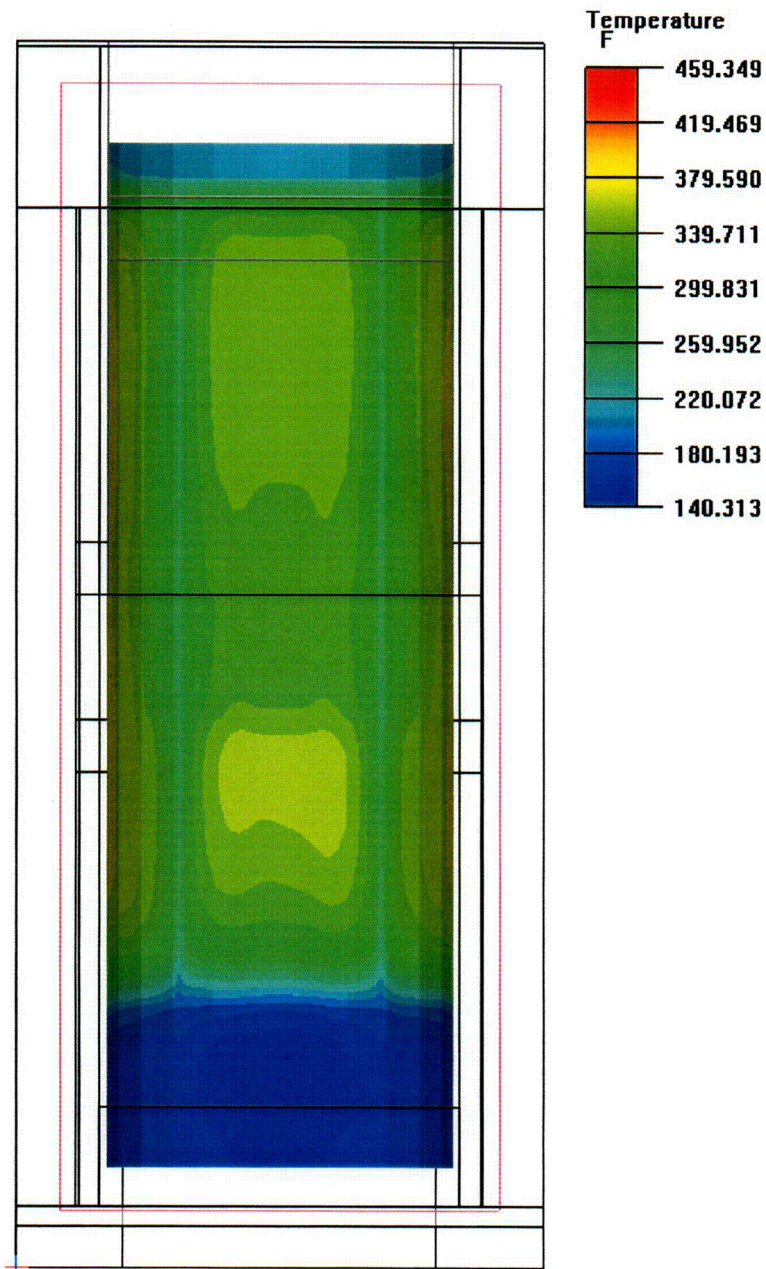


Figure 4-12 - Temperature Distribution On DSC, Bottom View, Normal Hot Storage Condition
(Note: Front face of AHSM module is at top of figure)

A TRANSNUCLEAR

PROJECT NO:	SCE-23	REVISION:	2
CALCULATION NO:	SCE-23.0410	PAGE:	31 of 65

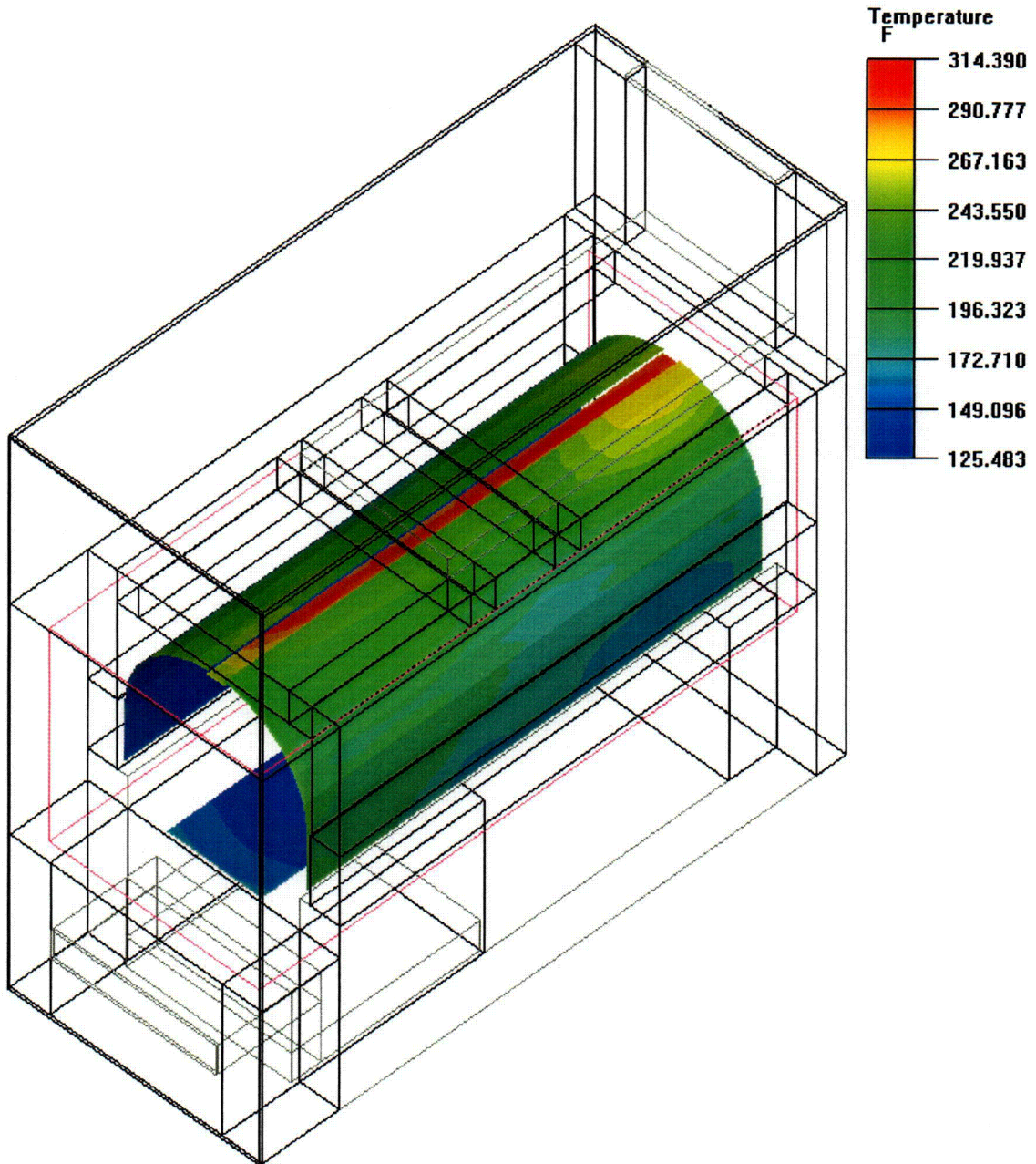


Figure 4-13 - Temperature Distribution On Heat Shield Surfaces, Normal Hot Storage Condition

C11

A TRANSNUCLEAR

PROJECT NO: SCE-23	REVISION: 2
CALCULATION NO: SCE-23.0410	PAGE: 32 of 65

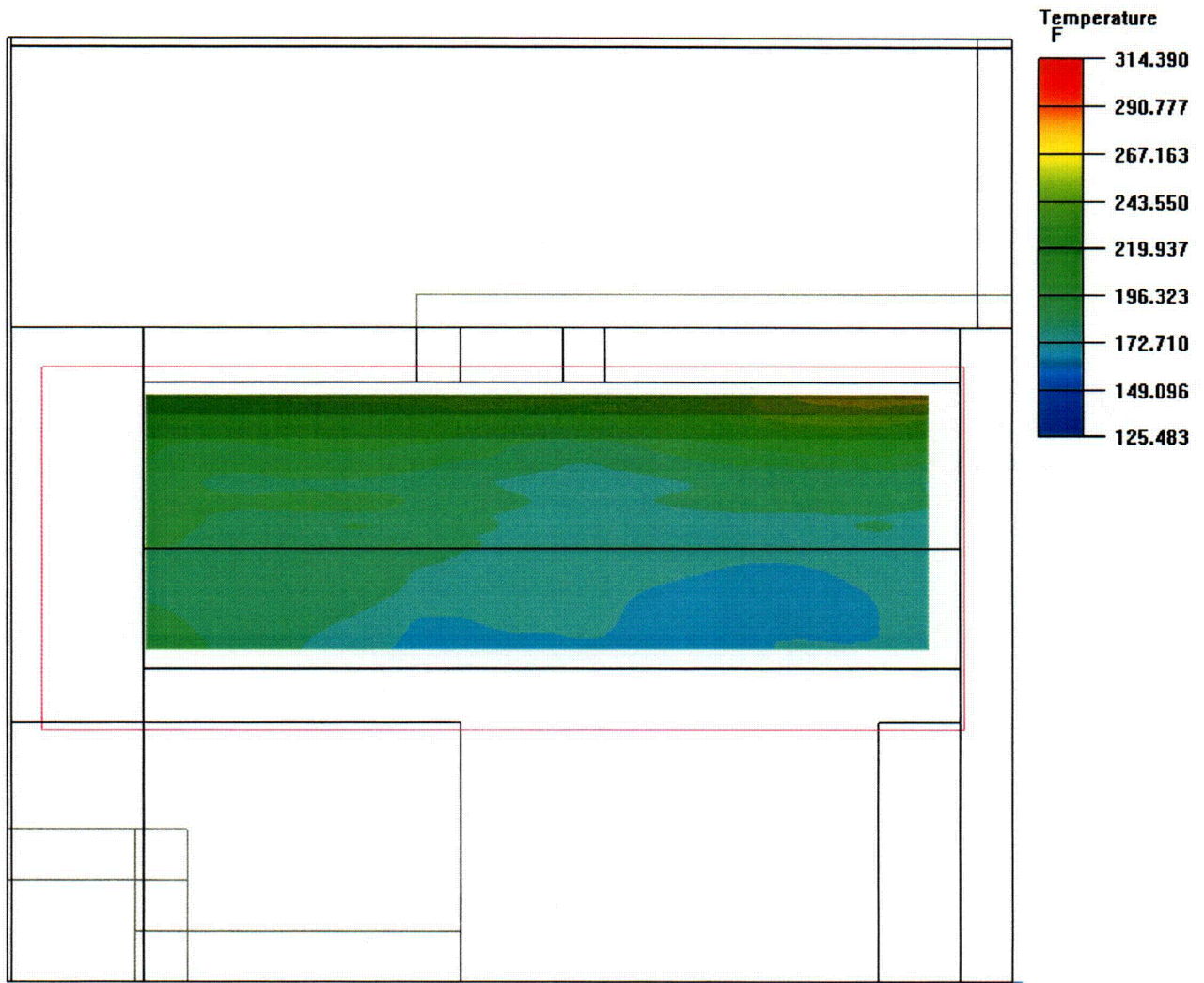


Figure 4-14 - Elevation View Of Temperature Distribution On Heat Shield, Normal Hot Storage Condition

(Note: Front face of AHSM module is at the top of the figure)

C12

A TRANSNUCLEAR

PROJECT NO: SCE-23	REVISION: 2
CALCULATION NO: SCE-23.0410	PAGE: 33 of 65

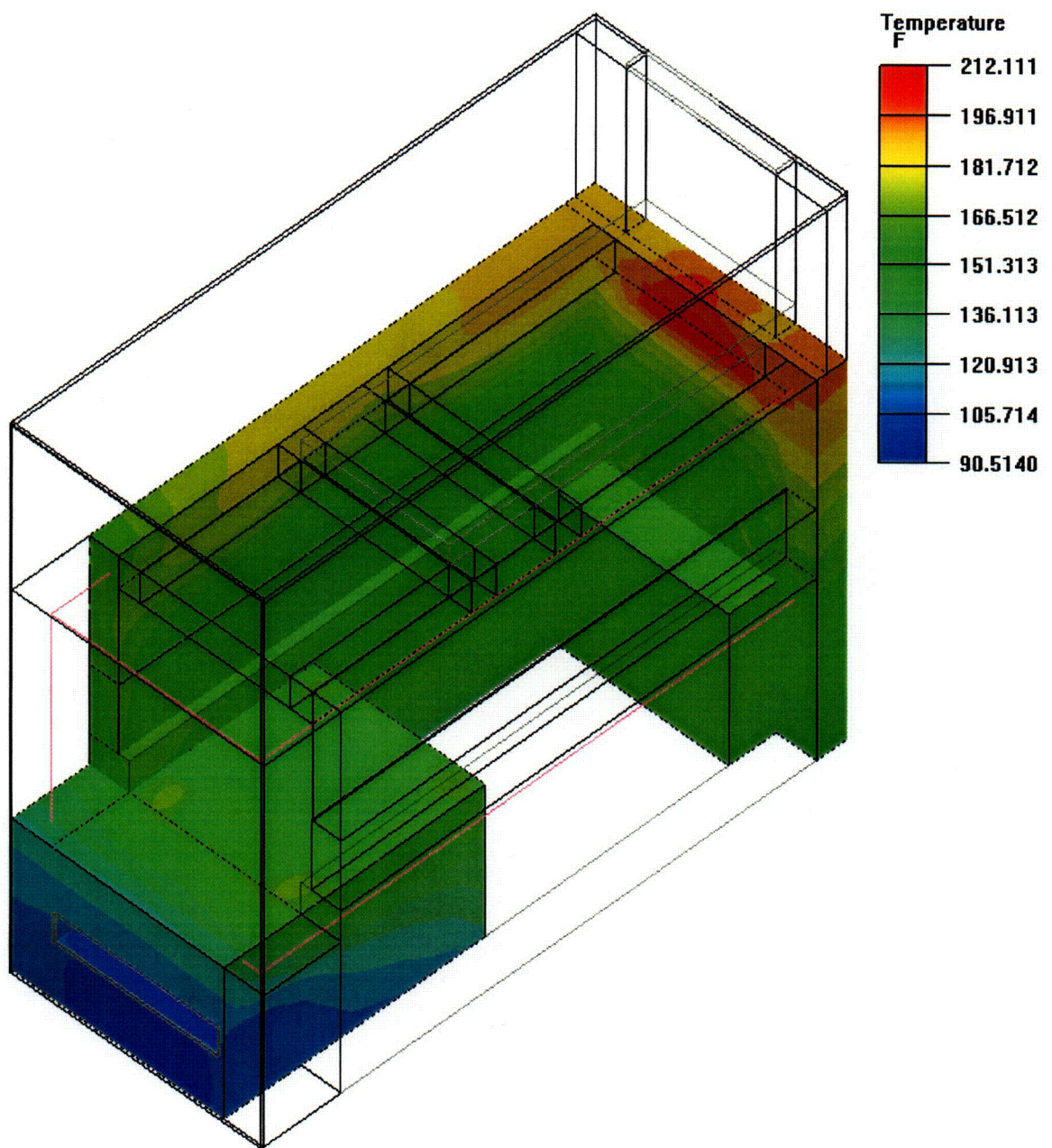


Figure 4-15 - Temperature Distribution On Concrete Surfaces Of Base Unit, Normal Hot Storage Condition

C13

A TRANSNUCLEAR

PROJECT NO:	SCE-23	REVISION:	2
CALCULATION NO:	SCE-23.0410	PAGE:	34 of 65

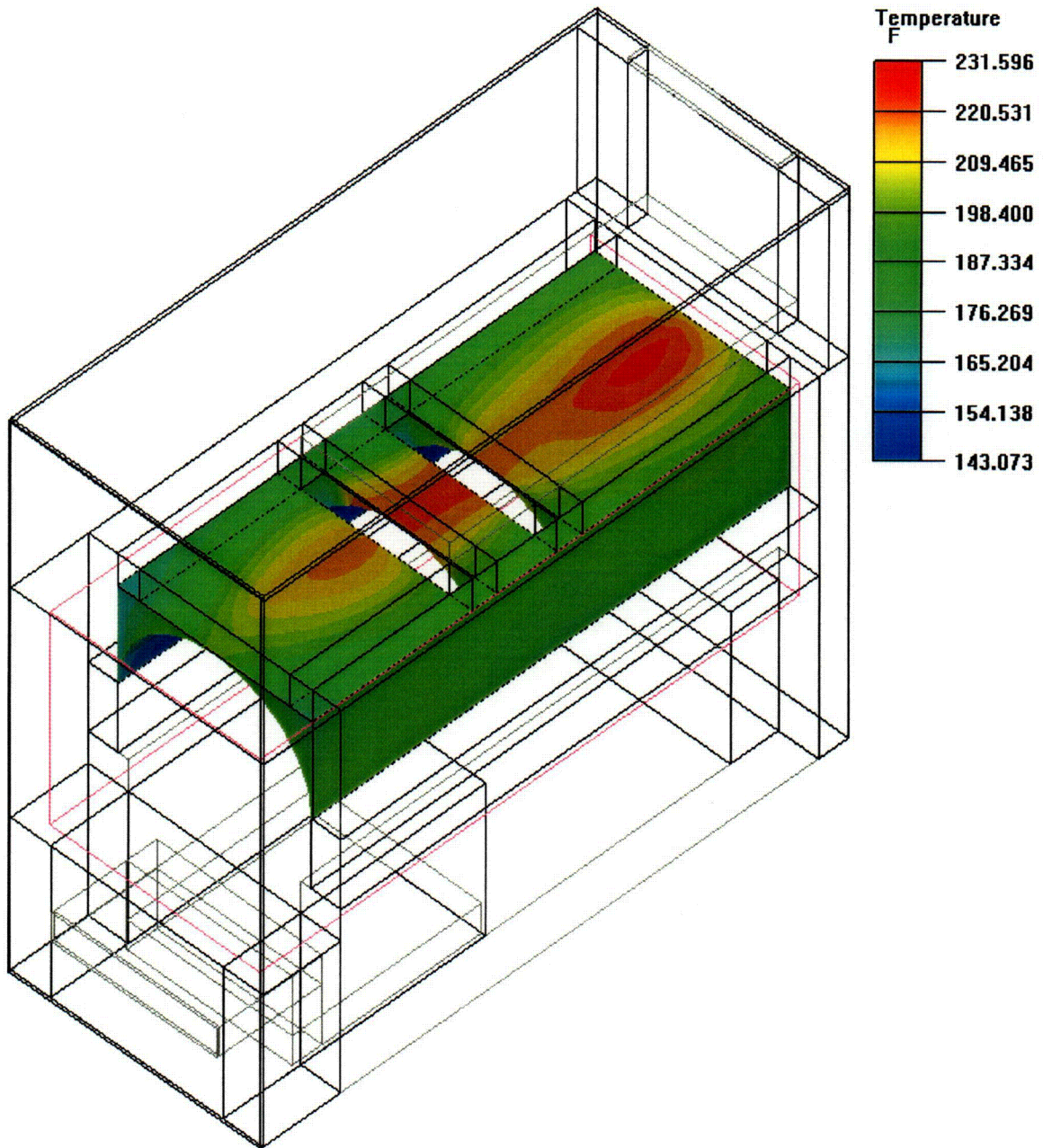


Figure 4-16 - Temperature Distribution On Concrete Vault Surfaces, Normal Hot Storage Condition

C14

PROJECT NO: SCE-23	REVISION: 2
CALCULATION NO: SCE-23.0410	PAGE: 35 of 65

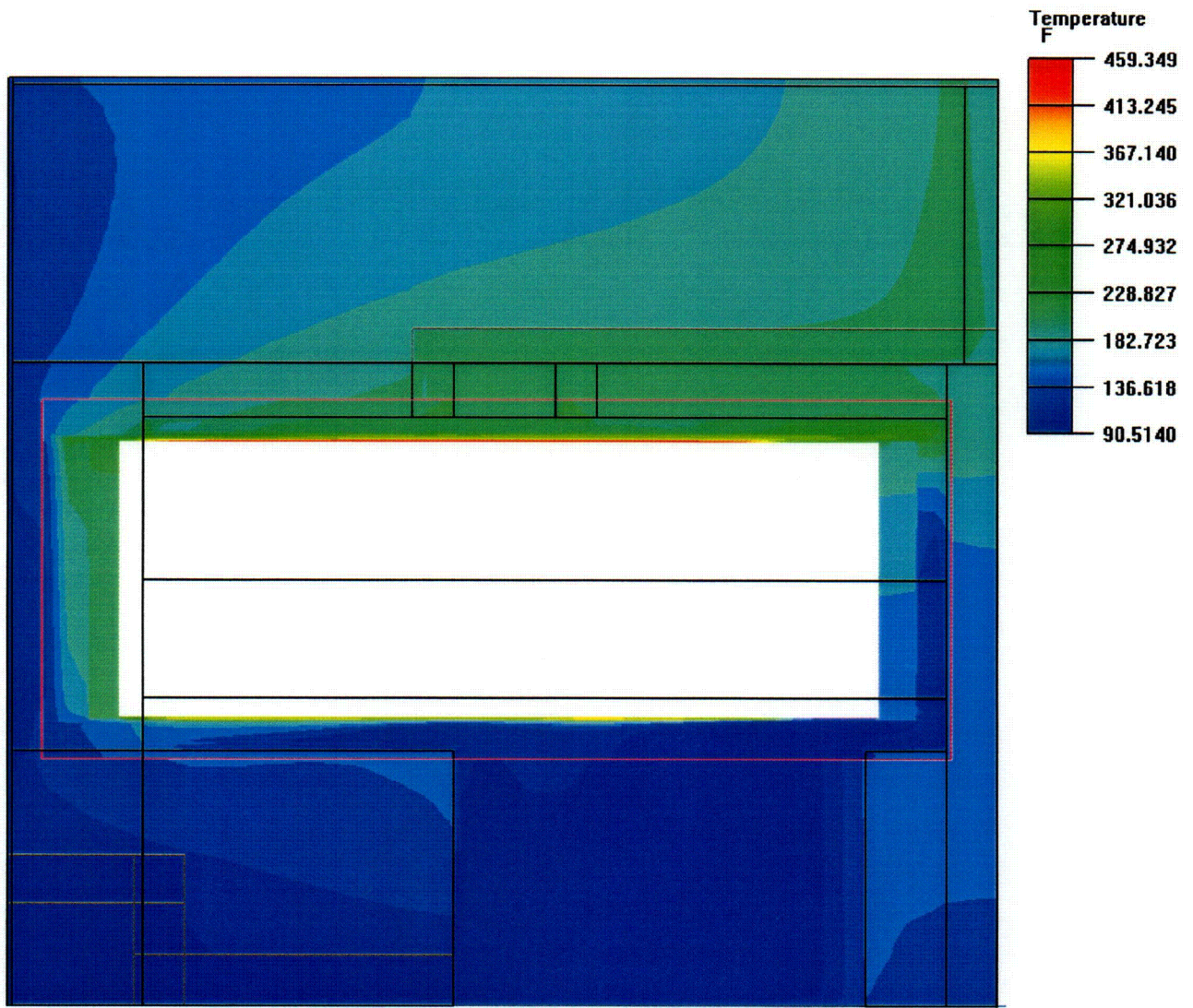


Figure 4-17 - Module Centerline Temperature Profile, Including Airspace, Normal Hot Storage Condition

(Note: Front face of AHSM module is to the left)

Q15

A TRANSNUCLEAR

PROJECT NO: SCE-23	REVISION: 2
CALCULATION NO: SCE-23.0410	PAGE: 36 of 65

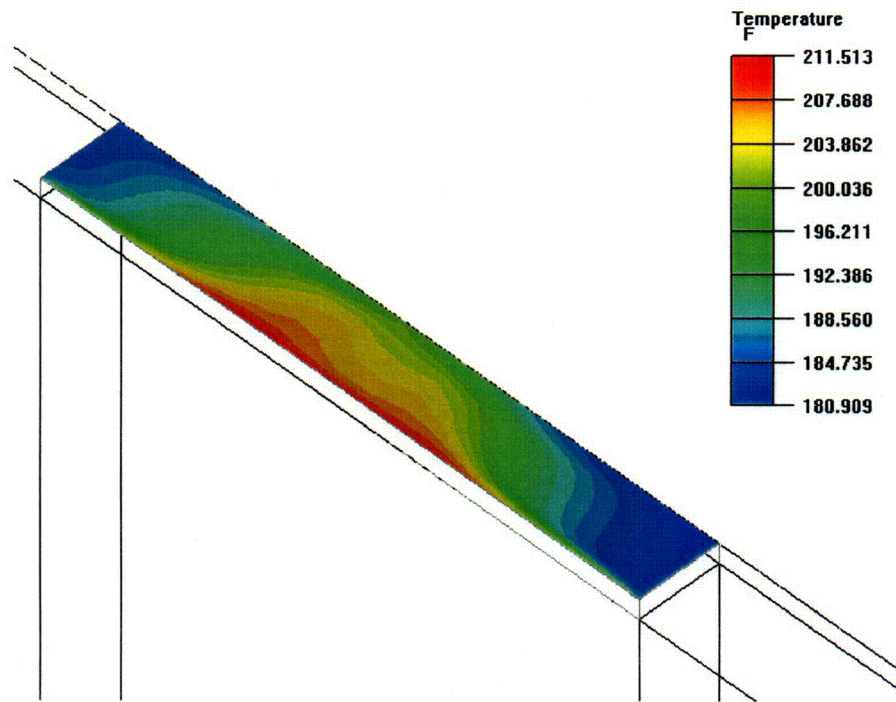


Figure 4-18 - Temperature Variation at Exhaust Vent, Normal Hot Storage Condition

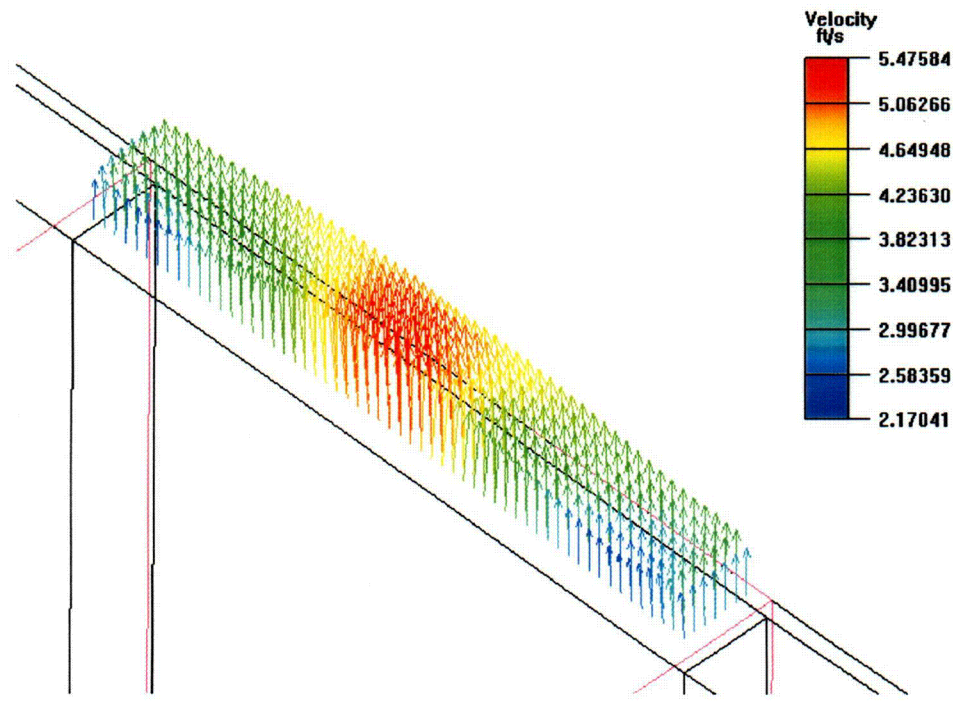


Figure 4-19 - Velocity Variation at Exhaust Vent, Normal Hot Storage Condition

C16

A TRANSCLEAR

PROJECT NO: SCE-23	REVISION: 2
CALCULATION NO: SCE-23.0410	PAGE: 37 of 65

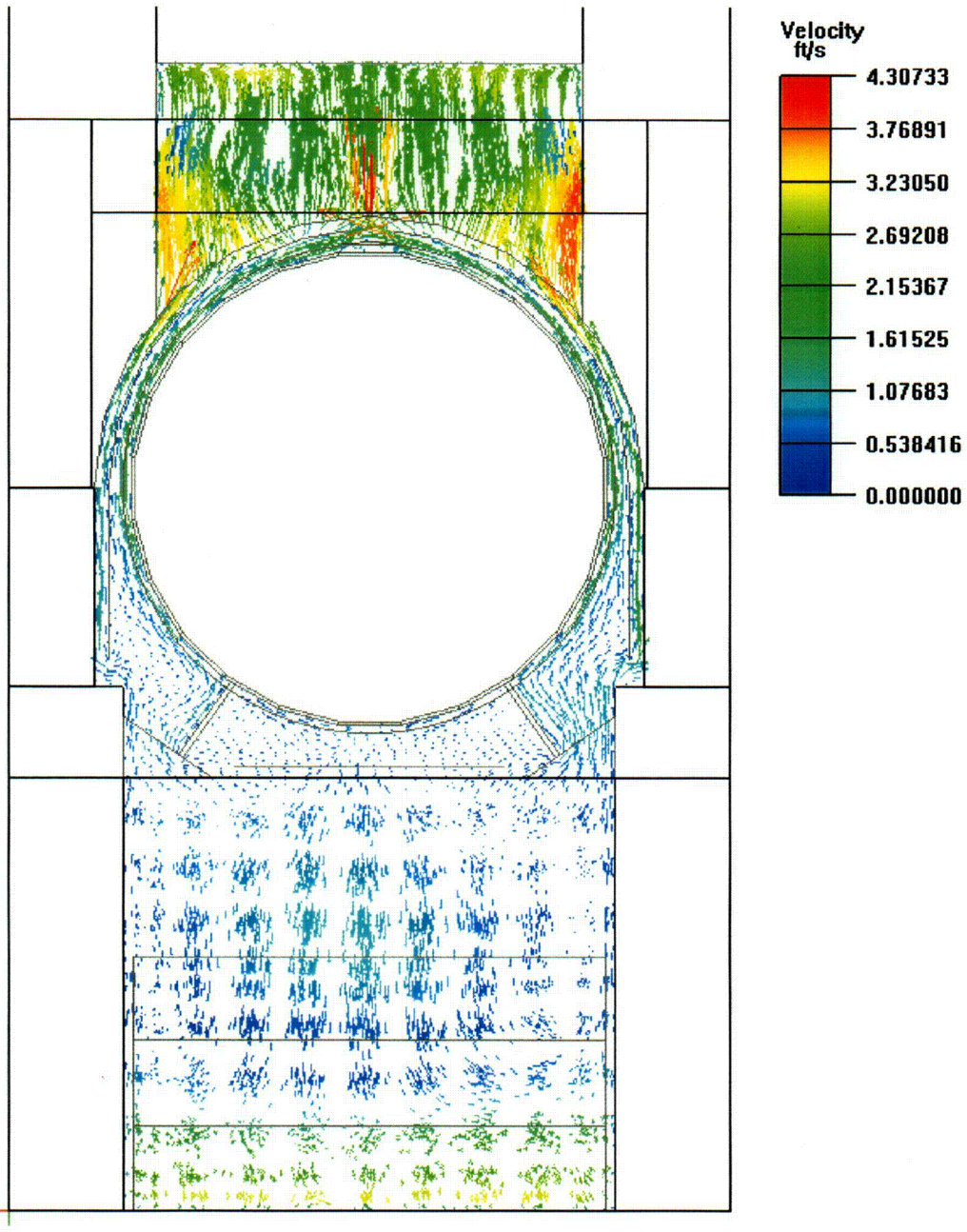


Figure 4-20 - Velocity Profile Along X-Y Plane Through AHSM, Normal Hot Storage Condition

(Note: Cut plane approx. 11'-3" from front face of AHSM, i.e., through rear vault duct)

C17

PROJECT NO: SCE-23	REVISION: 2
CALCULATION NO: SCE-23.0410	PAGE: 38 of 65

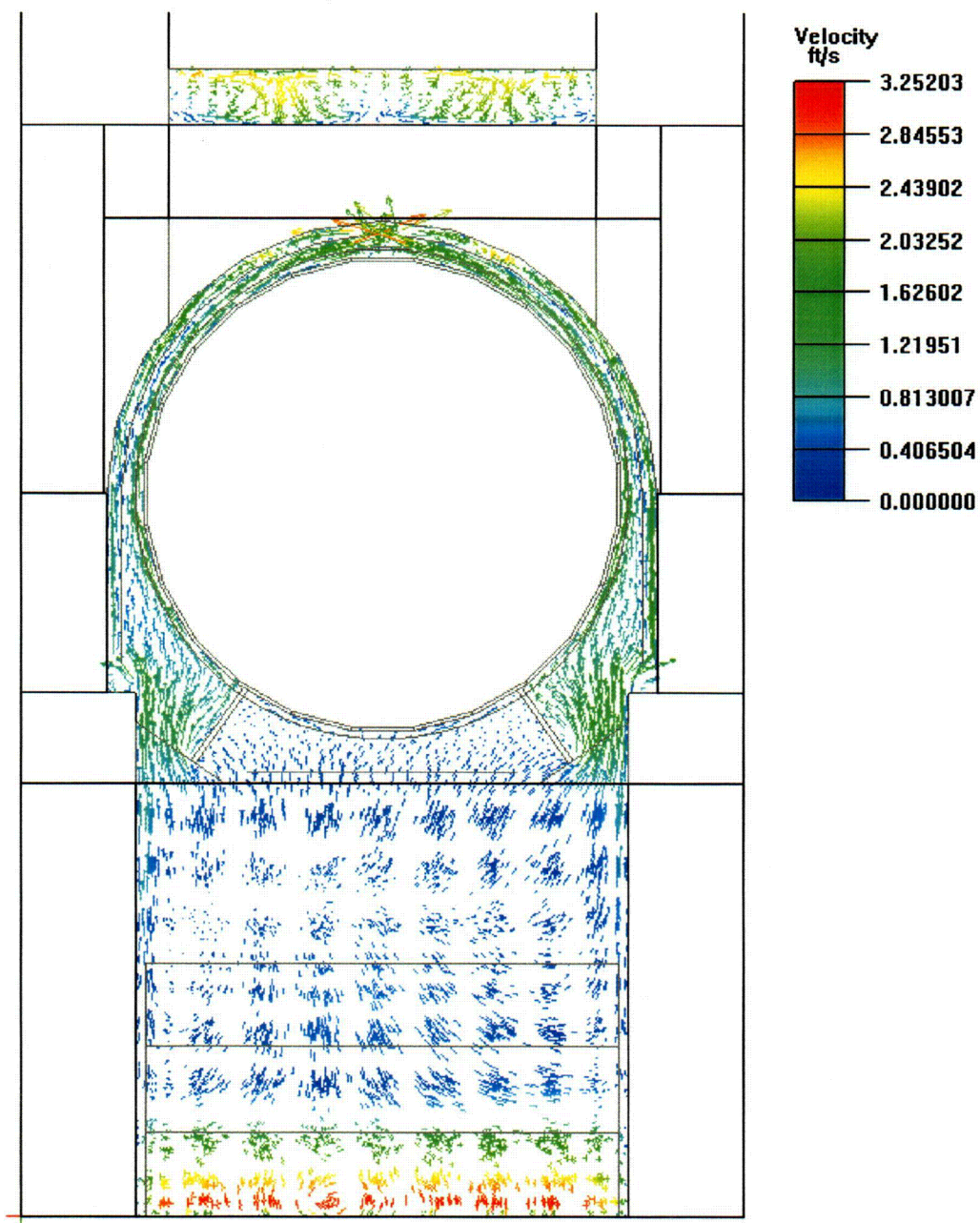


Figure 4-21 - Velocity Profile Along X-Y Plane Midway Through AHSM, Normal Hot Storage Condition

(Note: Cut plane approx. 9'-9.5" from front face of AHSM)

C18

A TRANSNUCLEAR

PROJECT NO: SCE-23	REVISION: 2
CALCULATION NO: SCE-23.0410	PAGE: 39 of 65

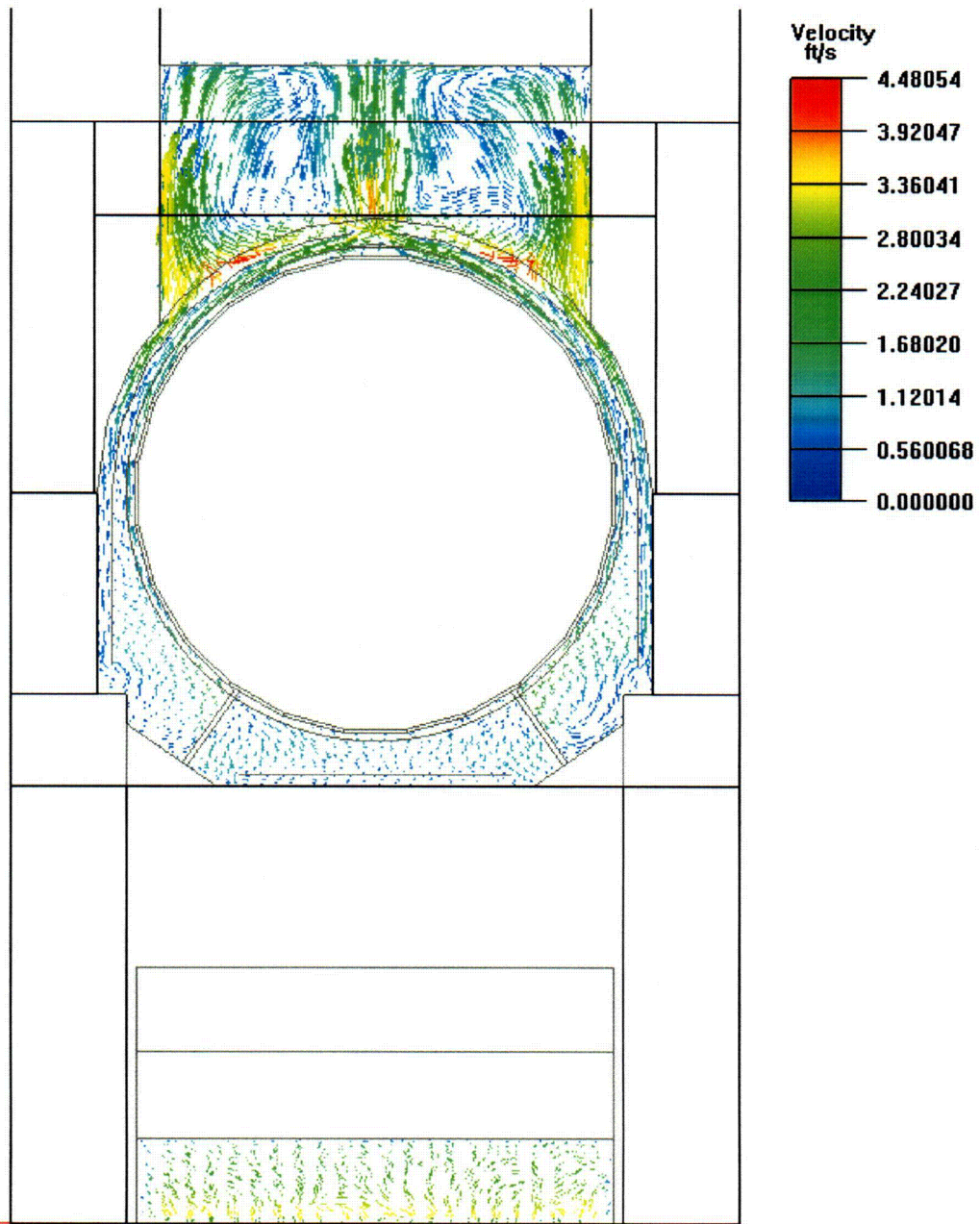


Figure 4-22 - Velocity Profile Along X-Y Plane Through AHSM, Normal Hot Storage Condition

(Note: Cut plane approx. 8'-5" from front face of AHSM, i.e., through front vault duct)

c19

PROJECT NO: SCE-23	REVISION: 2
CALCULATION NO: SCE-23.0410	PAGE: 40 of 65

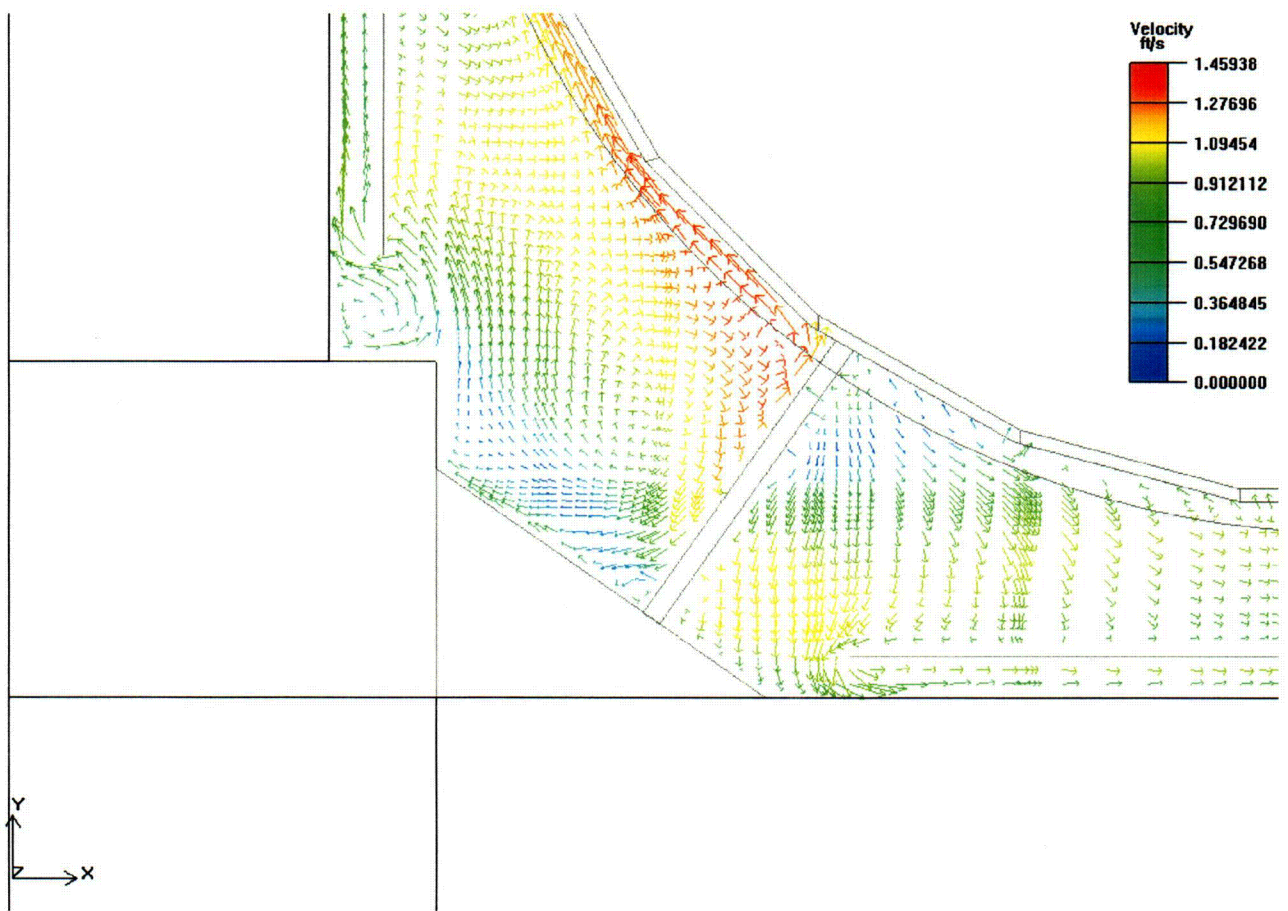
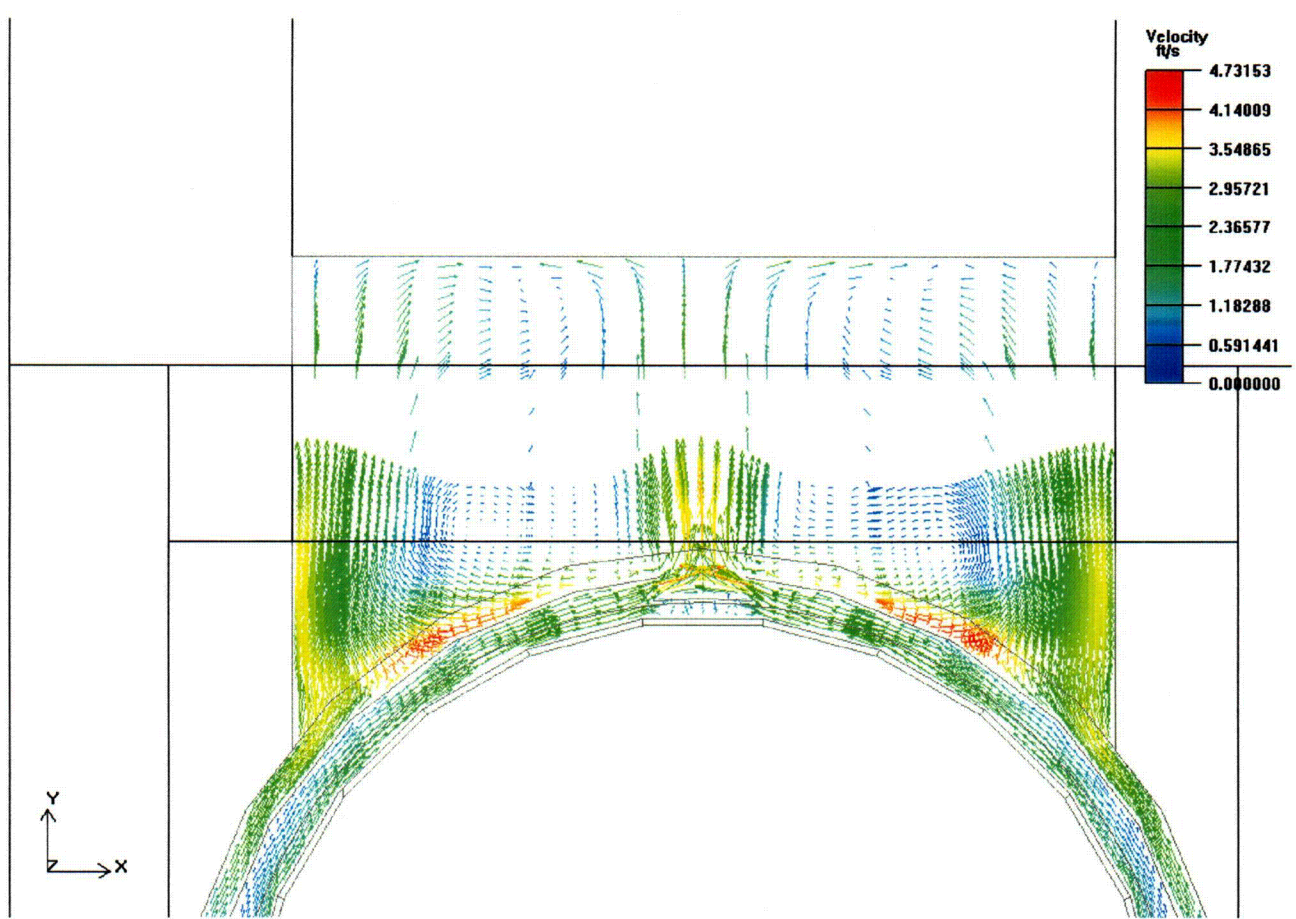


Figure 4-23 - Velocity Profile Along X-Y Plane In Vicinity Of DSC Support Structure, Normal Hot Storage Condition

(Note: Cut plane approx. 8'-5" from front face of AHSM, i.e., through front vault duct)

A TRANSNUCLEAR

PROJECT NO: SCE-23	REVISION: 2
CALCULATION NO: SCE-23.0410	PAGE: 41 of 65



**Figure 4-24 - Velocity Profile Along X-Y Plane In Vicinity Of Front Vault Duct,
Normal Hot Storage Condition**
(Note: Cut plane approx. 8'-5" from front face of AHSM, i.e., through front vault duct)

PROJECT NO: SCE-23	REVISION: 2
CALCULATION NO: SCE-23.0410	PAGE: 42 of 65

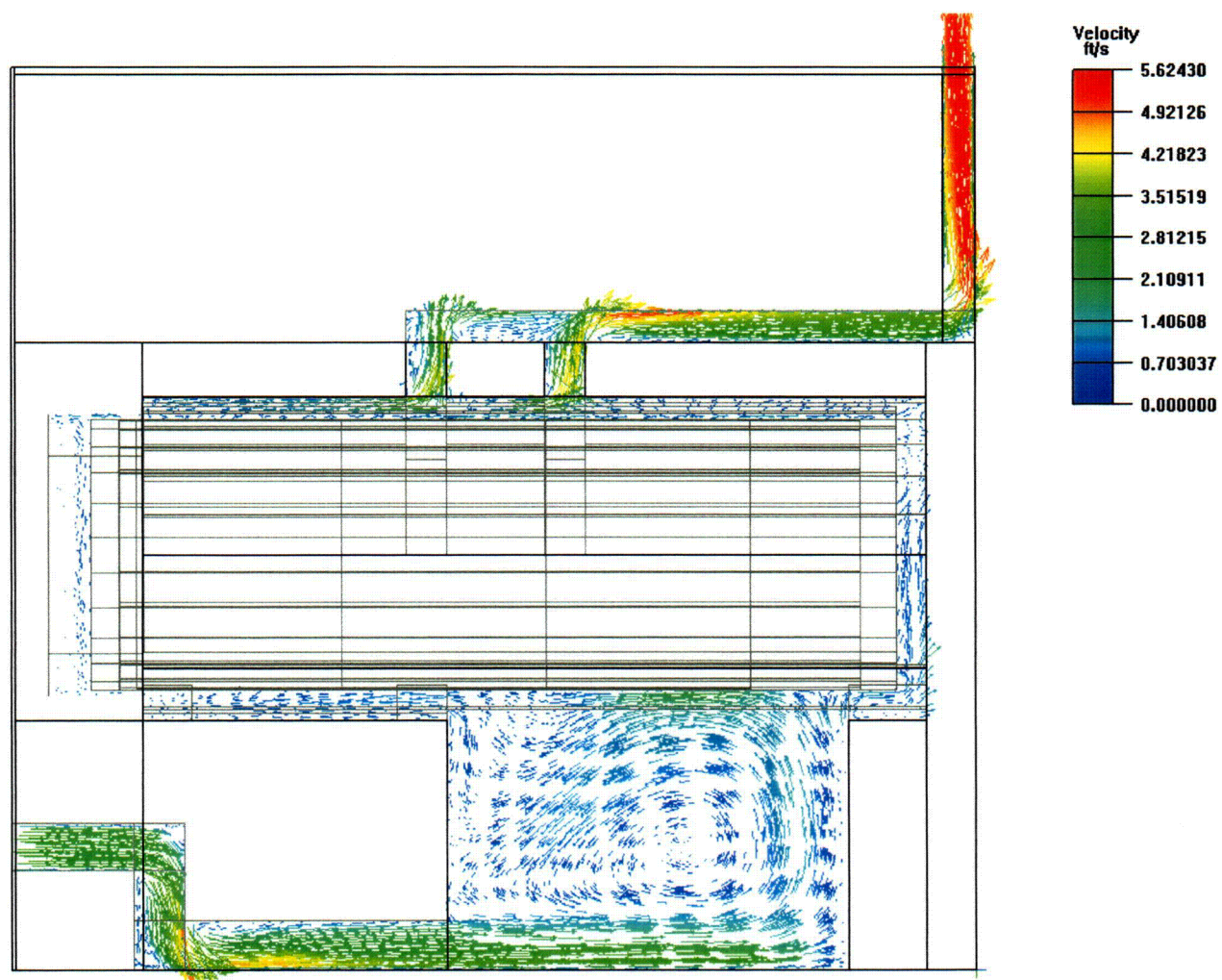
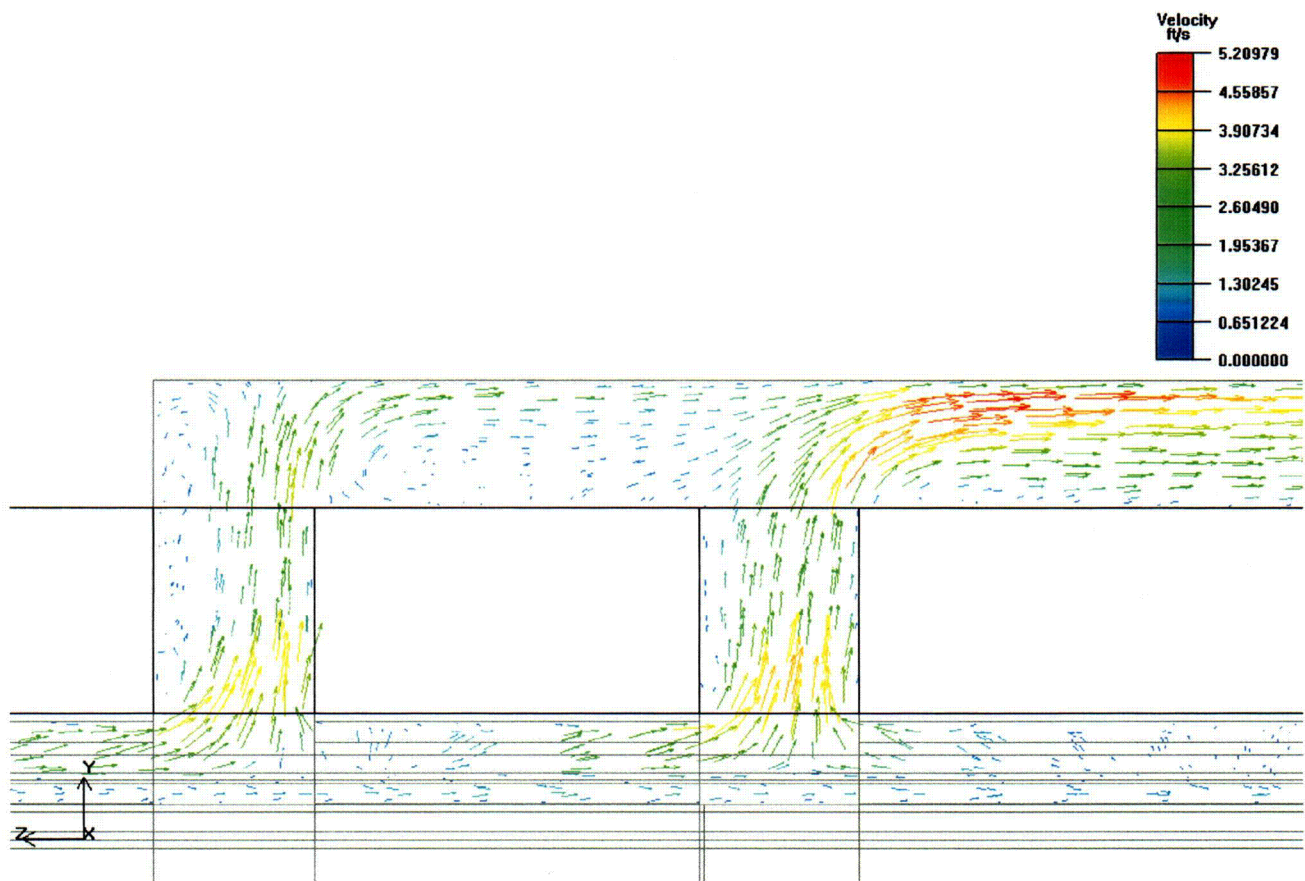


Figure 4-25 - Velocity Profile Along Y-Z Plane At Center Of AHSM, Normal Hot Storage Condition

C 22

PROJECT NO: SCE-23	REVISION: 2
CALCULATION NO: SCE-23.0410	PAGE: 43 of 65



**Figure 4-26 - Velocity Profile Along Y-Z Plane In Vicinity Of Vault Roof Ducts,
Normal Hot Storage Condition**

A TRANSNUCLEAR

PROJECT NO: SCE-23	REVISION: 2
CALCULATION NO: SCE-23.0410	PAGE: 44 of 65

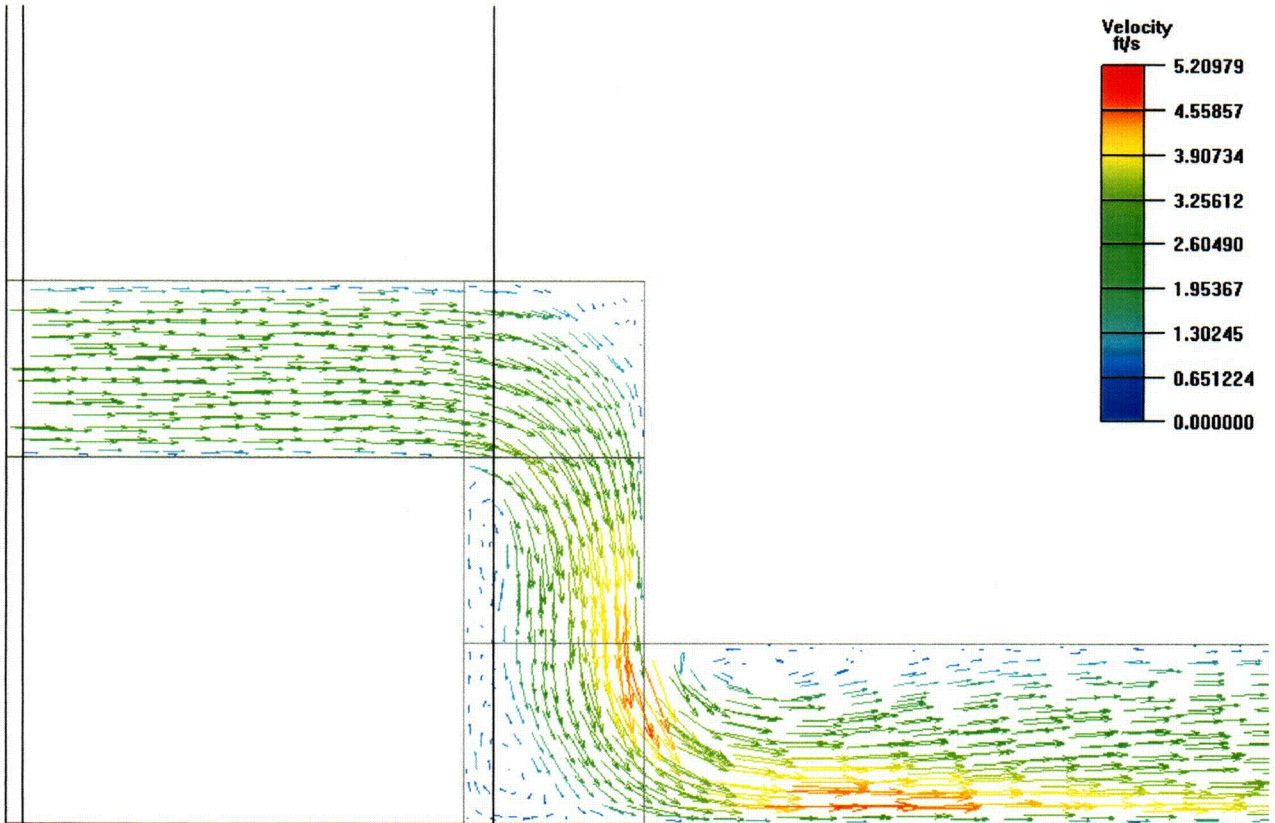


Figure 4-27 - Velocity Profile Along Y-Z Plane Approximately 22" From Edge Of AHSM, Normal Hot Storage Condition

PROJECT NO: SCE-23	REVISION: 2
CALCULATION NO: SCE-23.0410	PAGE: 45 of 65

4.3 Thermal Analysis at Off-Normal Cold Ambient Condition

Figure 4-28 to Figure 4-35 present a summary of the surface temperature distributions predicted for the analyzed decay heat loading of 24 kW within the DSC and the off-normal cold day condition (i.e., -40°F ambient air temperature with no insolation). The temperature variation over the surface of the DSC follows the same general pattern seen for the normal hot conditions of storage presented in Section 4.2. As seen from Figure 4-28 to Figure 4-30, the maximum surface temperature predicted under this condition is 359°F at the top of the DSC, approximately 276°F at the side of the DSC (see Figure 4-29), and 278°F at the bottom of the DSC (see Figure 4-30). In comparison, the [6.1] analysis predicts DSC shell temperatures of 271°F and 233°F at the top and bottom of the DSC shell, respectively.

Figure 4-31 illustrates the temperature profile on the heat shields within the AHSM module. A maximum temperature of 180°F occurs on the inner heat shield at the top of the vault, while the peak temperature on the upper heat shield at the top of the vault is predicted to be 136°F. In comparison, the [6.1] analysis predicts a peak heat shield temperature of 87°F. The elevation view of the temperature distribution in the heat shield illustrated in Figure 4-32 shows the expected results of higher temperatures with increased elevation. As with the results presented in Section 4.2, the variation in temperature from back to front on the heat shield reflects the computed distribution of airflow over the DSC.

Figure 4-33 depicts the temperature distribution over a portion of the concrete walls of the base unit, while Figure 4-34 illustrates the temperature distribution over the vault portion of the module. The analysis predicts a peak concrete temperature of 61°F at the back wall and 80°F at the inside surface of the vault. The [6.1] analysis predicts a peak temperature of 56°F for these same locations. The maximum temperature of 170°F for the DSC support structure occurs at the point of contact between the rails and the DSC temperature. Since the [6.1] analysis did not specifically model the support structure components, it conservatively assumed its peak temperature along the bottom of the DSC of 233°F for the maximum support rail temperature.

Figure 4-35 presents an elevation view of the predicted temperature distribution along an axial plane through the module. The figure reflects the expected temperature distribution given the general airflow paths and the presence of the DSC. Figure 4-36 presents the temperature variation at the exhaust outlet and Figure 4-37 illustrates the variation in the flow velocity at the same location. The peak temperature at the exhaust vent is 52°F, while the average exhaust air temperature is 40°F. As such, the predicted air temperature rise through the AHSM is $40 - (-40) = 80^\circ\text{F}$ vs. the 72.7°F predicted by the [6.1] analysis. The predicted airflow rate is 1.10 lbm/sec.

Figure 4-38 to Figure 4-40 present the flow velocity profiles at selected locations within the AHSM module. Note that the velocity scale in each figure is re-scaled to span the range of velocities occurring within the depicted view. Figure 4-38 illustrates the profiles along an x-y plane through the middle of the second (i.e., rear) vertical flow duct out of the AHSM vault. The profile shows the expected trend of relatively low flow velocity over most of the AHSM with regions of re-circulation

A

TRANSNUCLEAR

PROJECT NO: SCE-23	REVISION: 2
CALCULATION NO: SCE-23.0410	PAGE: 46 of 65

within the lower plenum and between the support rails, increasing flow velocity around the DSC due to the smaller flow space, and the maximum velocity achieved at exit flow ducts. A similar flow distribution is noted in Figure 4-39 which illustrates the predicted flow profile at an x-y plane through the middle of the first (i.e., front) vertical flow duct.

Figure 4-40 illustrates the flow profile along a y-z plane through the center of the module. The figure depicts the same general flow pattern as seen for the analysis of the normal hot condition of storage (see Section 4.2). The maximum flow velocity of approximately 4.9 feet per second occurs in the vertical exhaust duct at the rear of the module. As explained in Section 2.2, this peak velocity is conservative since the vertical exhaust channel is modeled 16" narrower than the actual dimension. As such, the actual peak flow velocity will be approximately 20% less or approximately 3.9 ft/sec.

A TRANSNUCLEAR

PROJECT NO: SCE-23	REVISION: 2
CALCULATION NO: SCE-23.0410	PAGE: 47 of 65

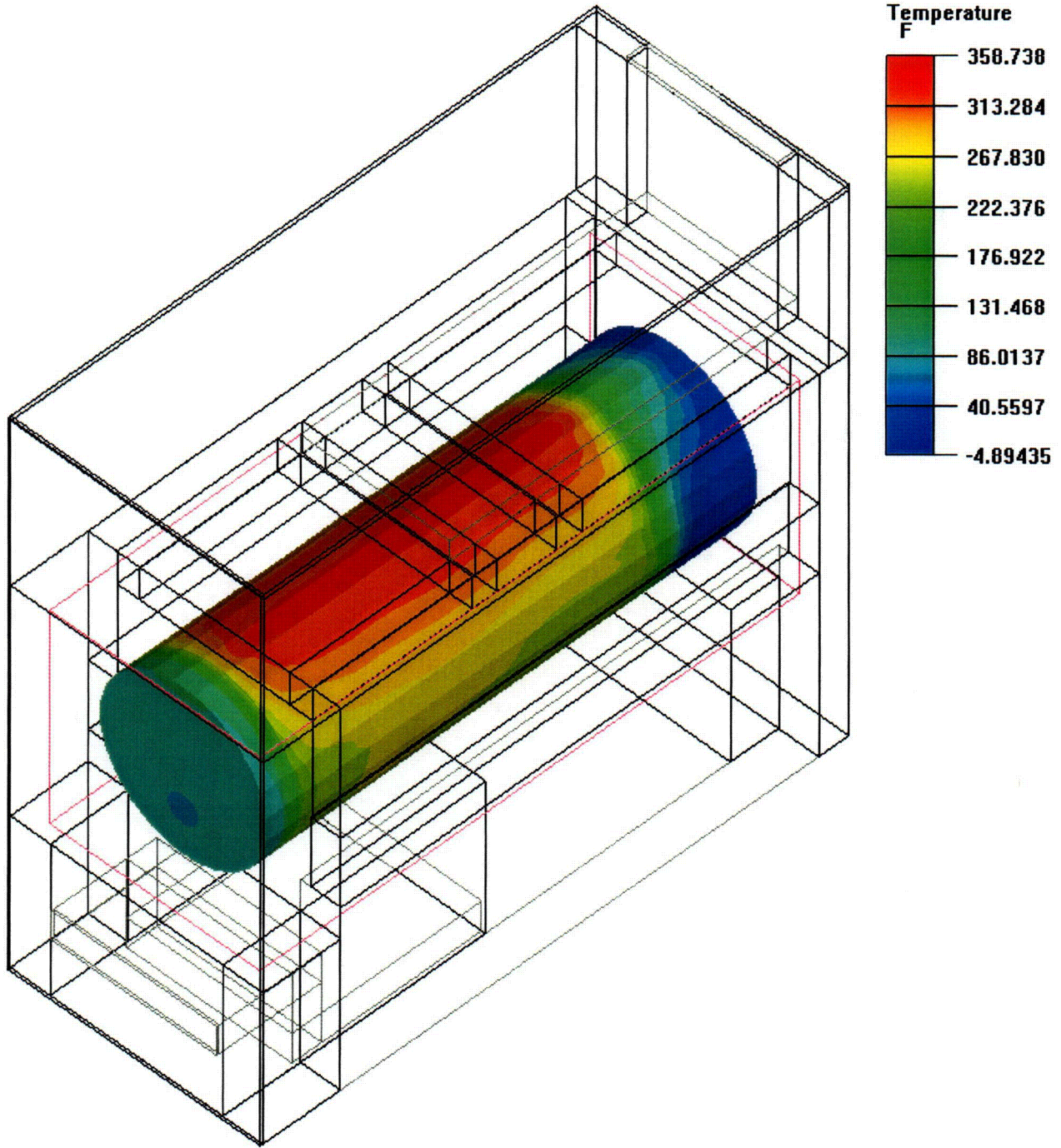


Figure 4-28 - Temperature Distribution On DSC Surface, Perspective View, Off-Normal Cold Storage Condition

A TRANSNUCLEAR

PROJECT NO: SCE-23	REVISION: 2
CALCULATION NO: SCE-23.0410	PAGE: 48 of 65

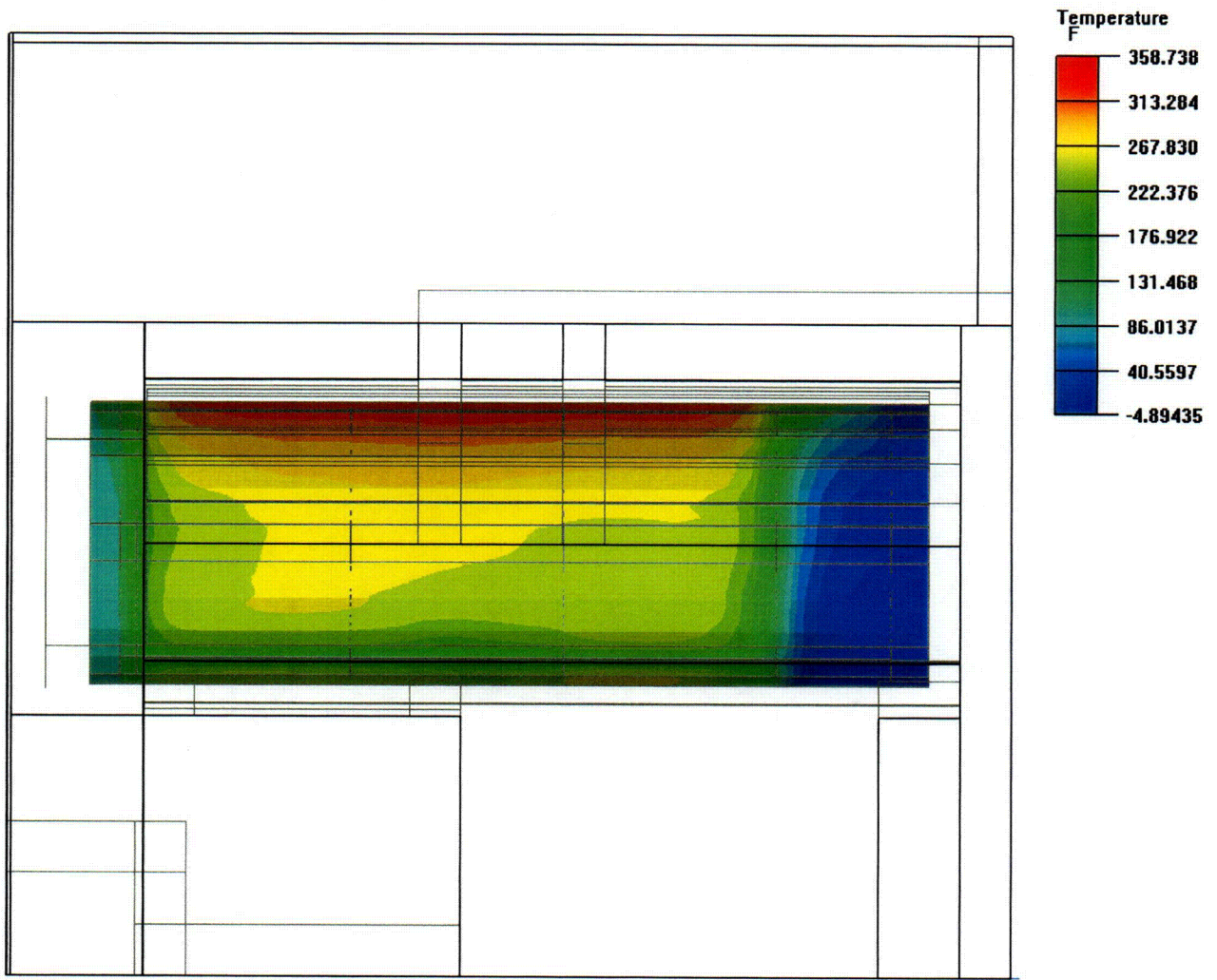


Figure 4-29 - Temperature Distribution On DSC, Side View, Off-Normal Cold Storage Condition

(Note: Front face of AHSM module is at left side of figure)

PROJECT NO: SCE-23	REVISION: 2
CALCULATION NO: SCE-23.0410	PAGE: 49 of 65

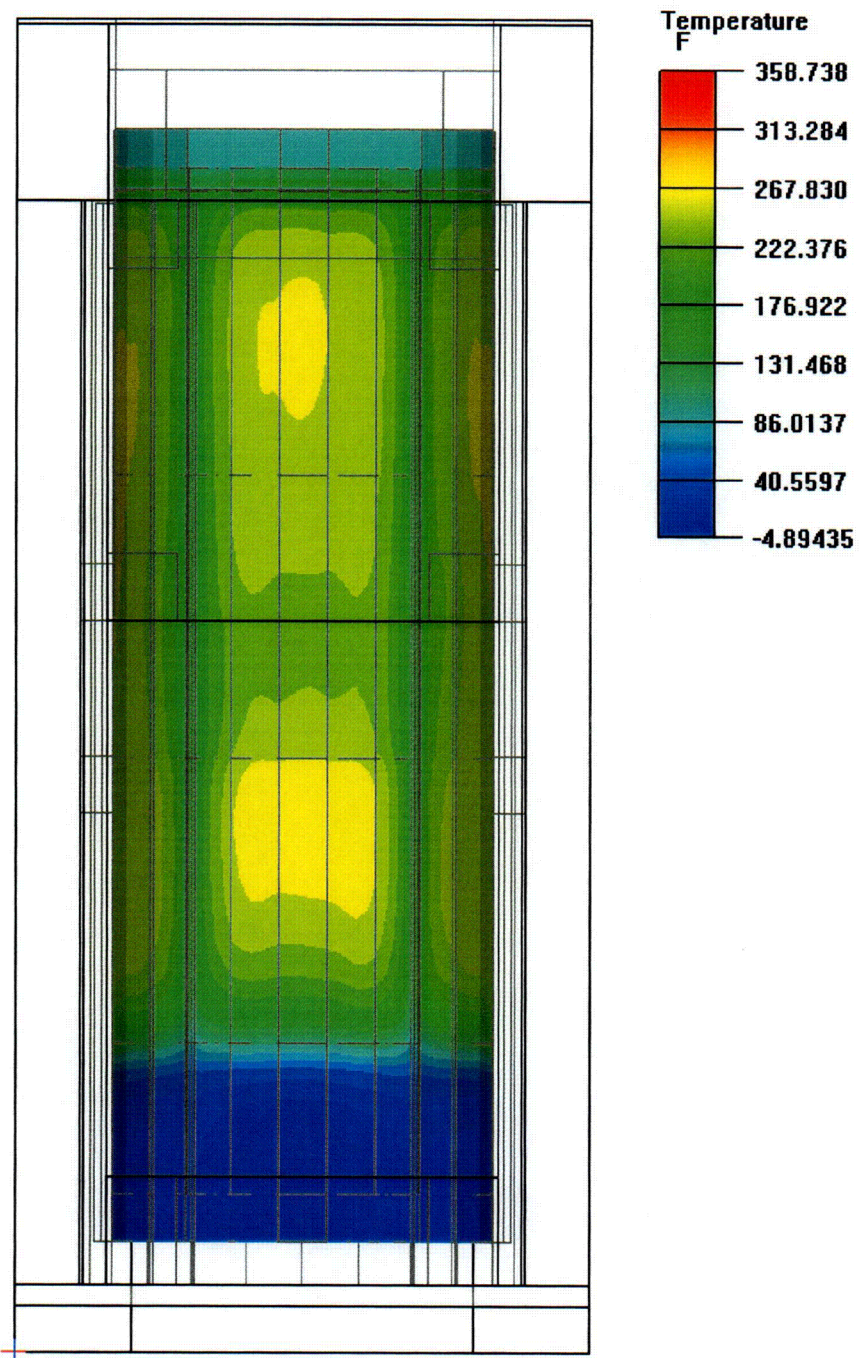


Figure 4-30 - Temperature Distribution On DSC, Bottom View, Off-Normal Cold Storage Condition

(Note: Front face of AHSM module is at top of figure)

C27

A TRANSNUCLEAR

PROJECT NO: SCE-23
CALCULATION NO: SCE-23.0410

REVISION: 2
PAGE: 50 of 65

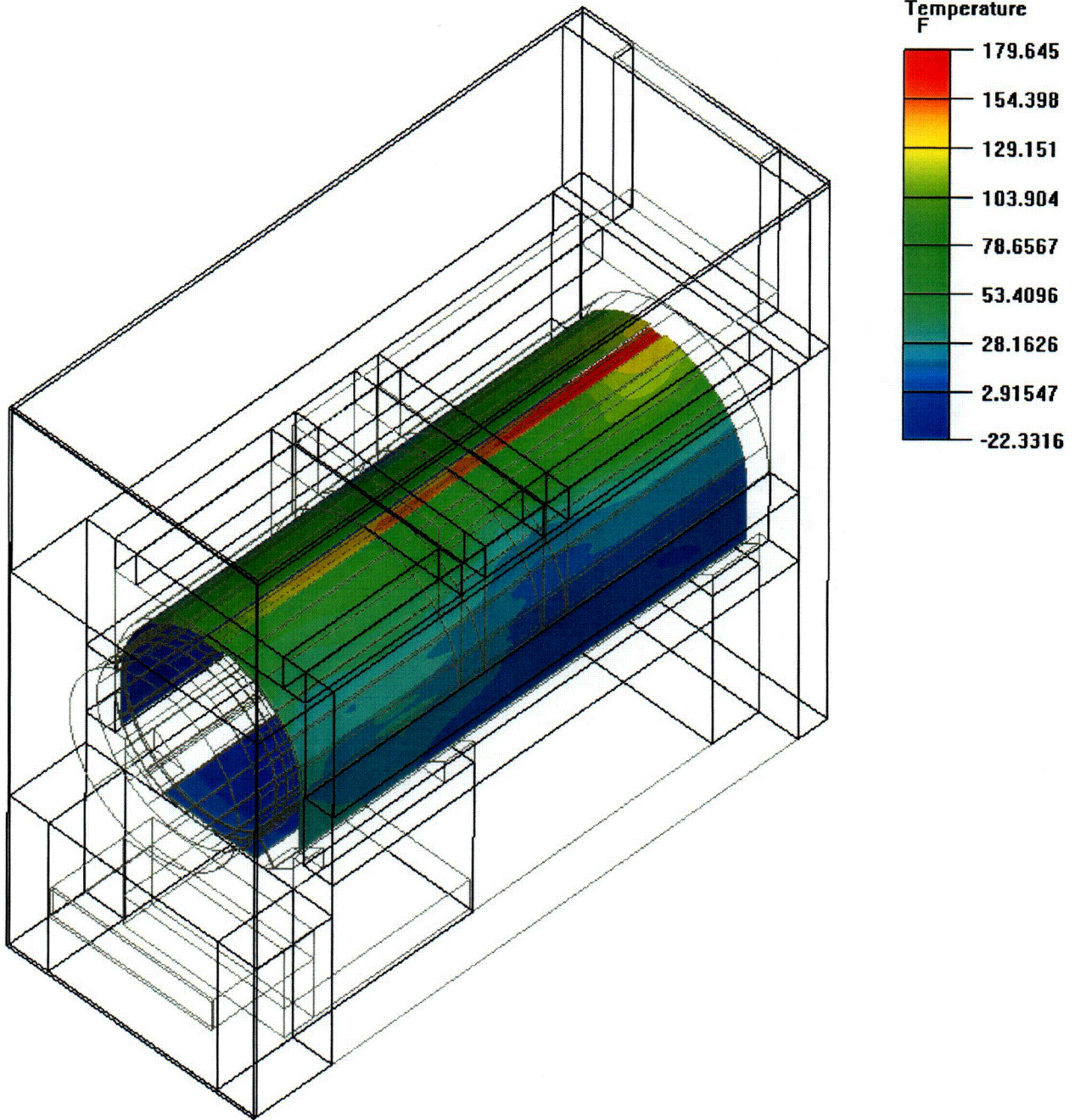


Figure 4-31 - Temperature Distribution On Heat Shield Surfaces, Off-Normal Cold Storage Condition

PROJECT NO: SCE-23	REVISION: 2
CALCULATION NO: SCE-23.0410	PAGE: 51 of 65

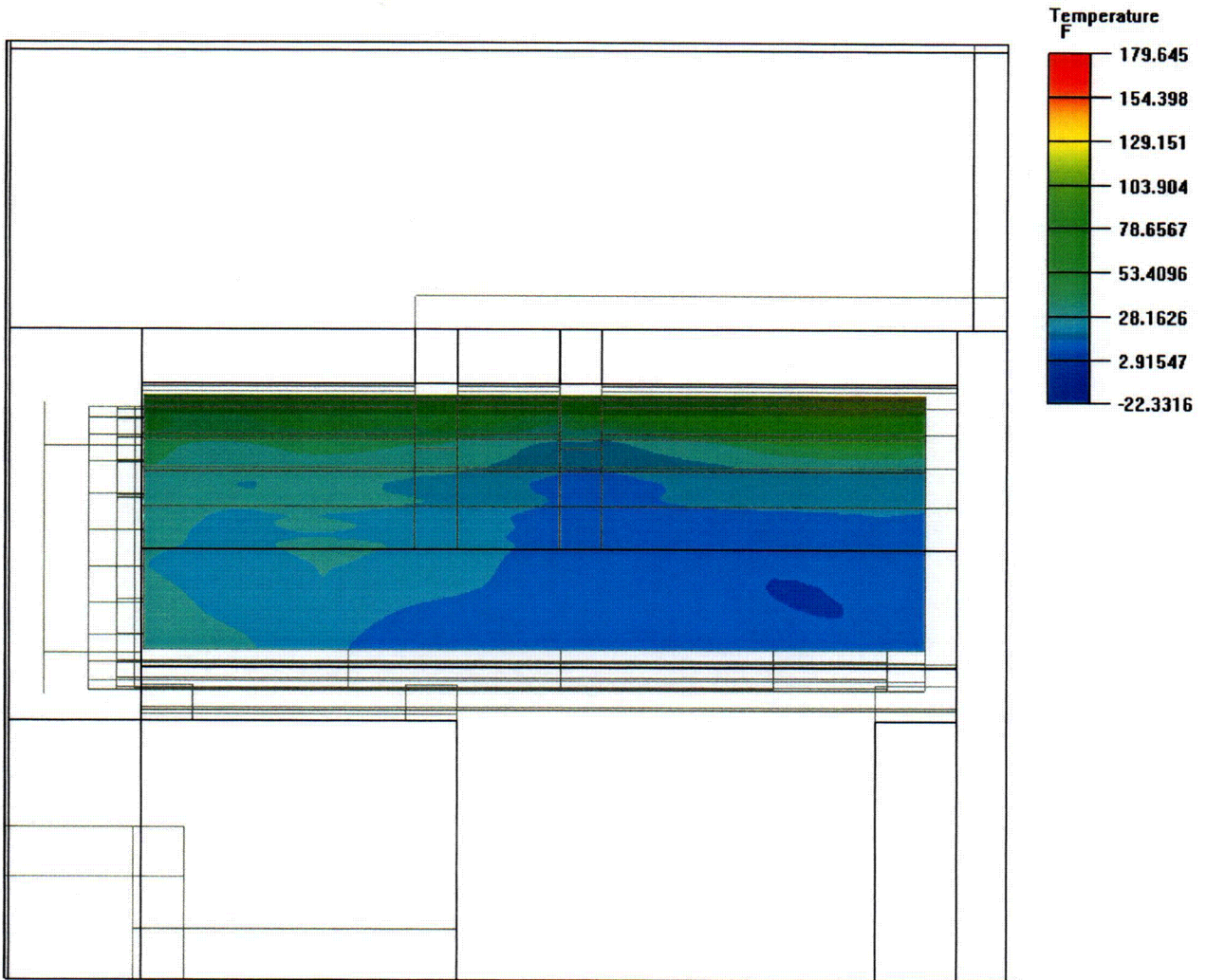


Figure 4-32 - Elevation View Of Temperature Distribution On Heat Shield, Off-Normal Cold Storage Condition

(Note: Front face of AHSM module is at the top of the figure)

A TRANSNUCLEAR

PROJECT NO: SCE-23
CALCULATION NO: SCE-23.0410

REVISION: 2
PAGE: 52 of 65

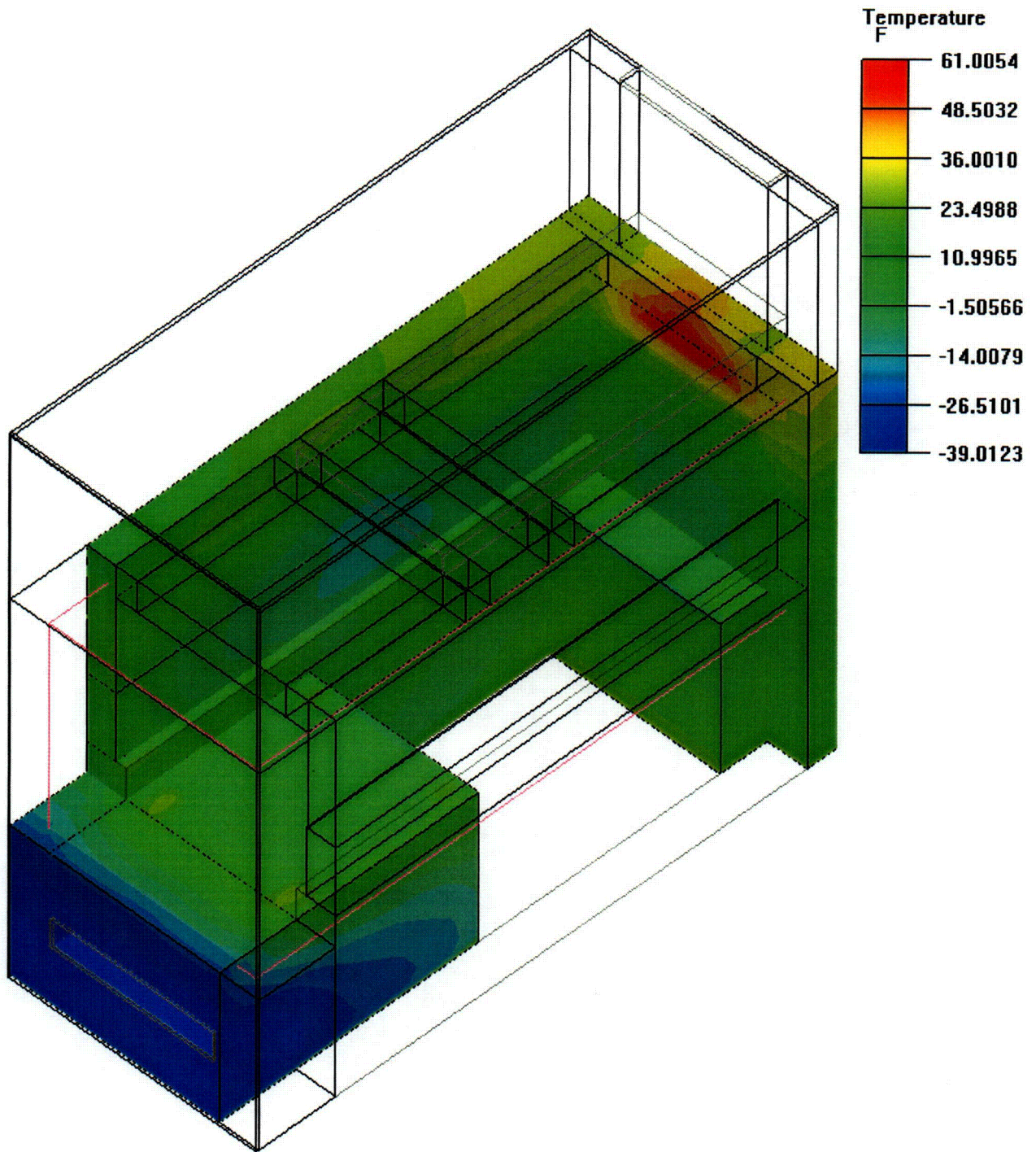


Figure 4-33 - Temperature Distribution On Concrete Surfaces Of Base Unit, Off-Normal Cold Storage Condition

A TRANSCLEAR

PROJECT NO: SCE-23
CALCULATION NO: SCE-23.0410

REVISION: 2
PAGE: 53 of 65

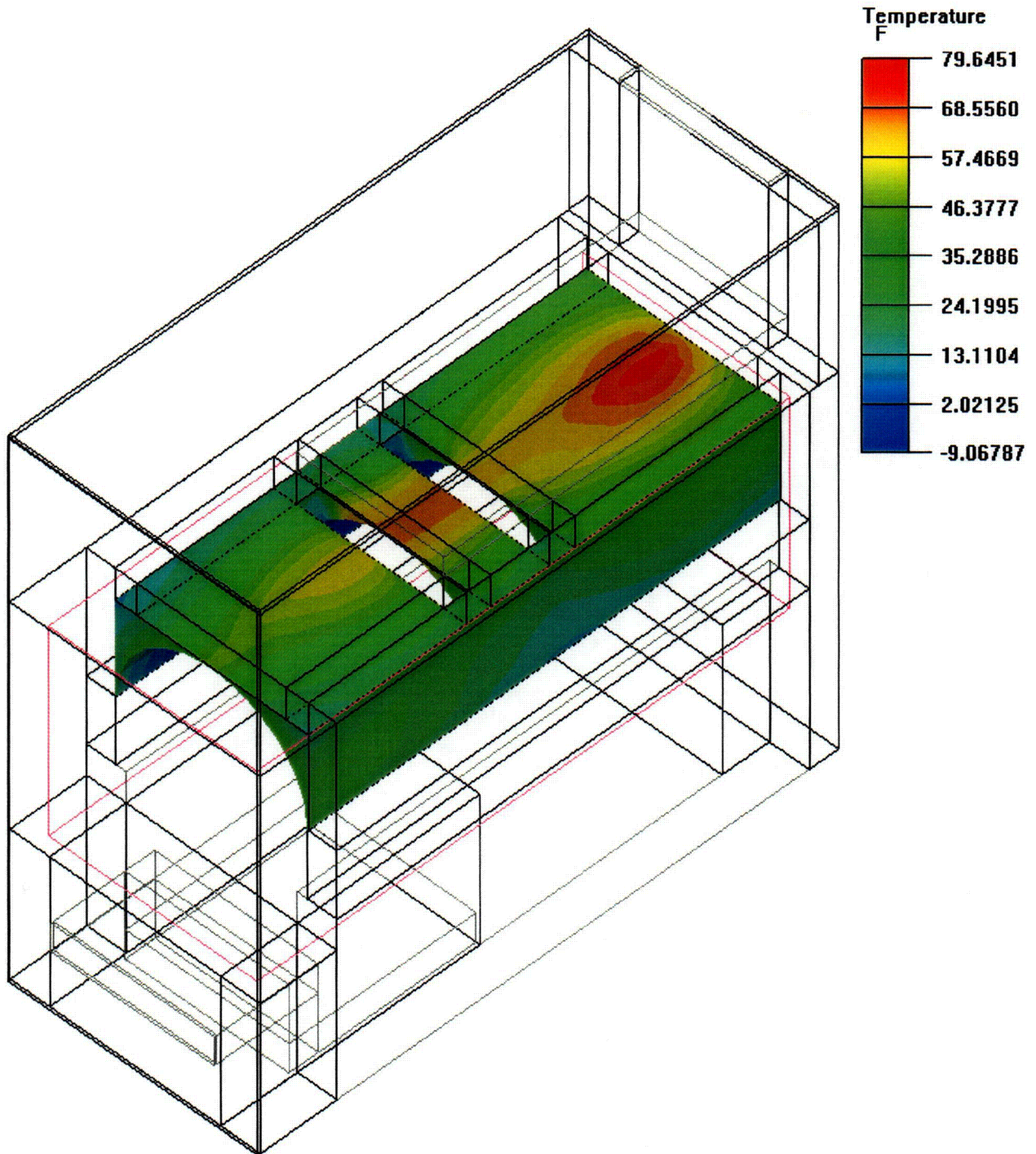


Figure 4-34 - Temperature Distribution On Concrete Vault Surfaces, Off-Normal Cold Storage Condition

PROJECT NO: SCE-23	REVISION: 2
CALCULATION NO: SCE-23.0410	PAGE: 54 of 65

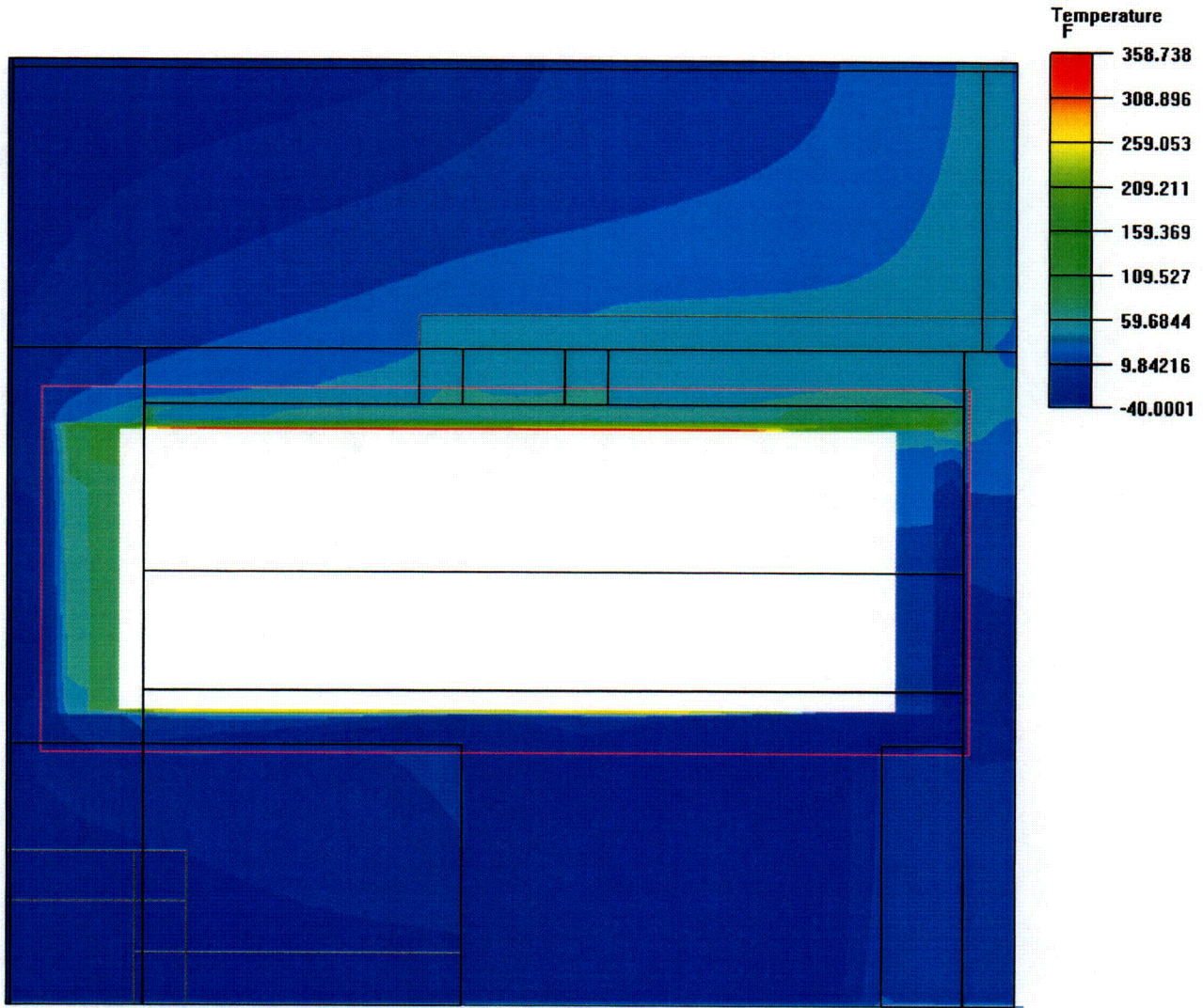


Figure 4-35 - Module Centerline Temperature Profile, Including Airspace, Off-Normal Cold Storage Condition

(Note: Front face of AHSM module is to the left)

A TRANSCLEAR

PROJECT NO: SCE-23	REVISION: 2
CALCULATION NO: SCE-23.0410	PAGE: 55 of 65

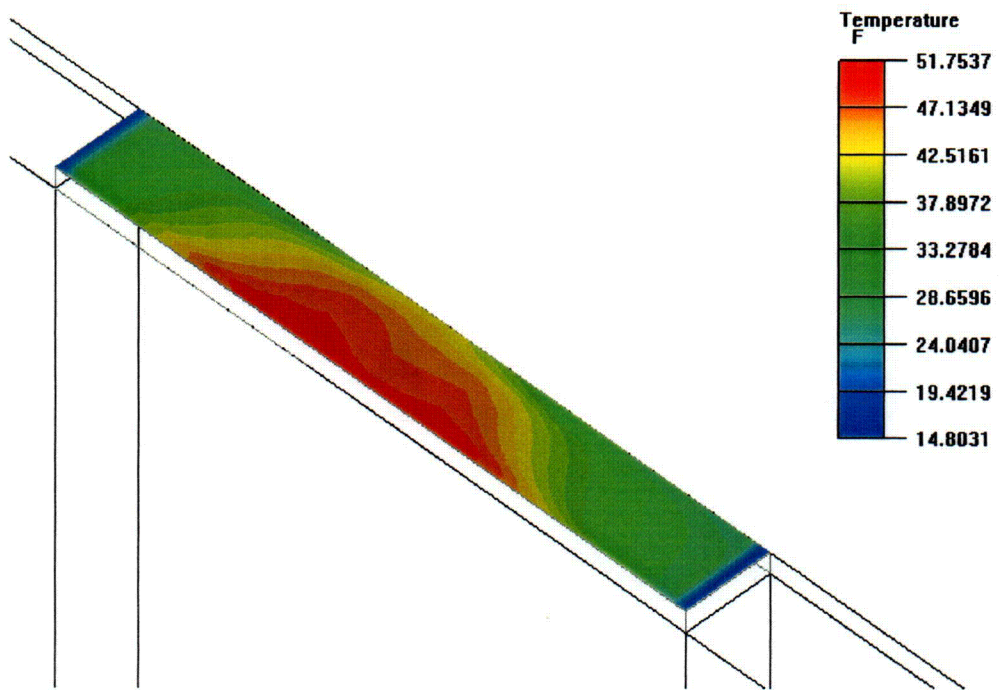


Figure 4-36 - Temperature Variation at Exhaust Vent, Off-Normal Cold Storage Condition

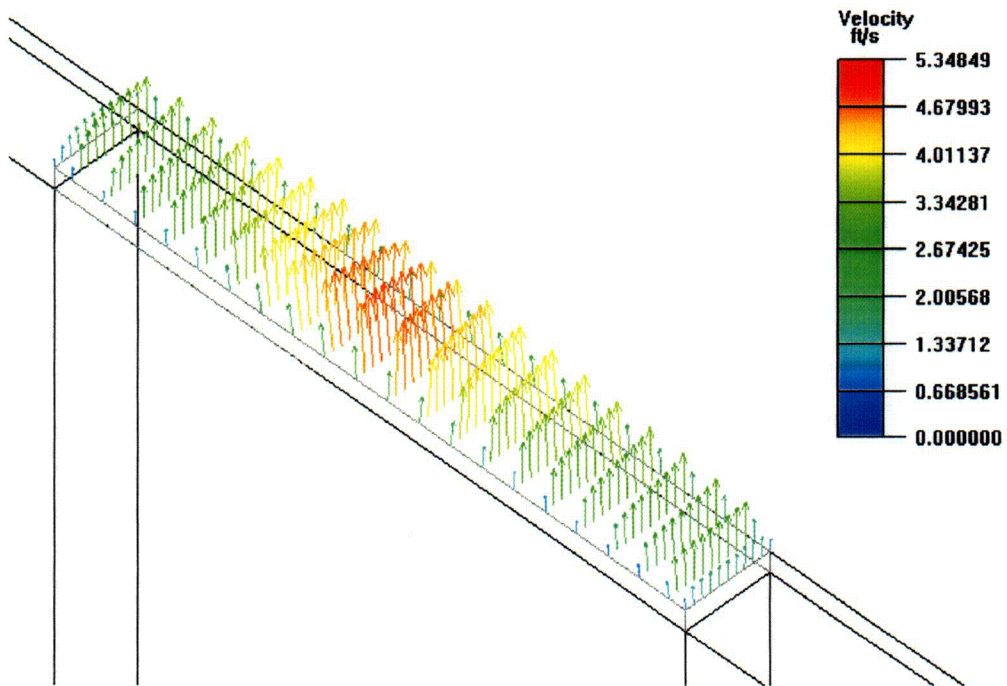


Figure 4-37 - Velocity Variation at Exhaust Vent, Off-Normal Cold Storage Condition

A TRANSNUCLEAR

PROJECT NO: SCE-23	REVISION: 2
CALCULATION NO: SCE-23.0410	PAGE: 56 of 65

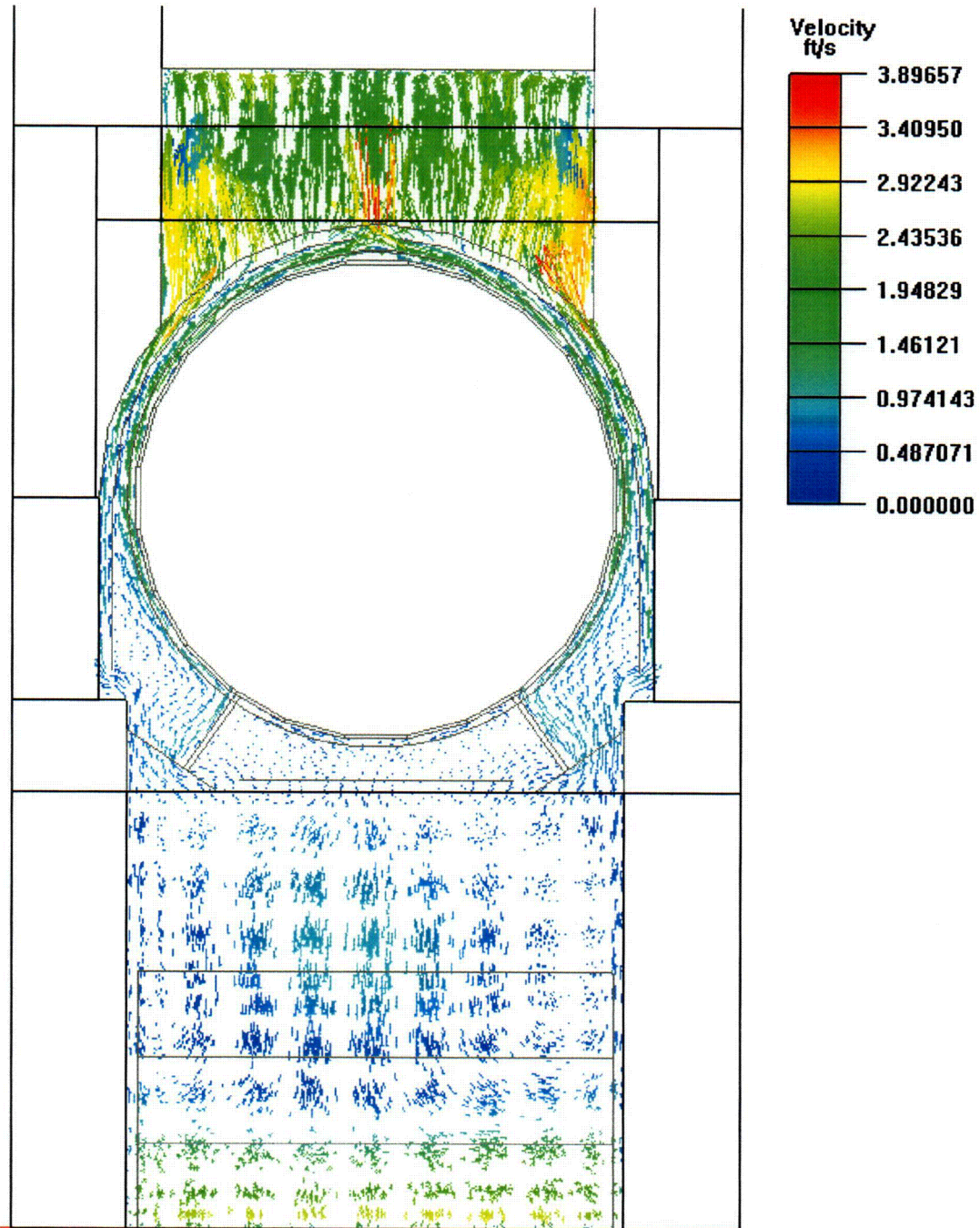


Figure 4-38 - Velocity Profile Along X-Y Plane Through AHSM, Off-Normal Cold Storage Condition

(Note: Cut plane approx. 11'-3" from front face of AHSM, i.e., through rear vault duct)

C34

A TRANSNUCLEAR

PROJECT NO: SCE-23	REVISION: 2
CALCULATION NO: SCE-23.0410	PAGE: 57 of 65

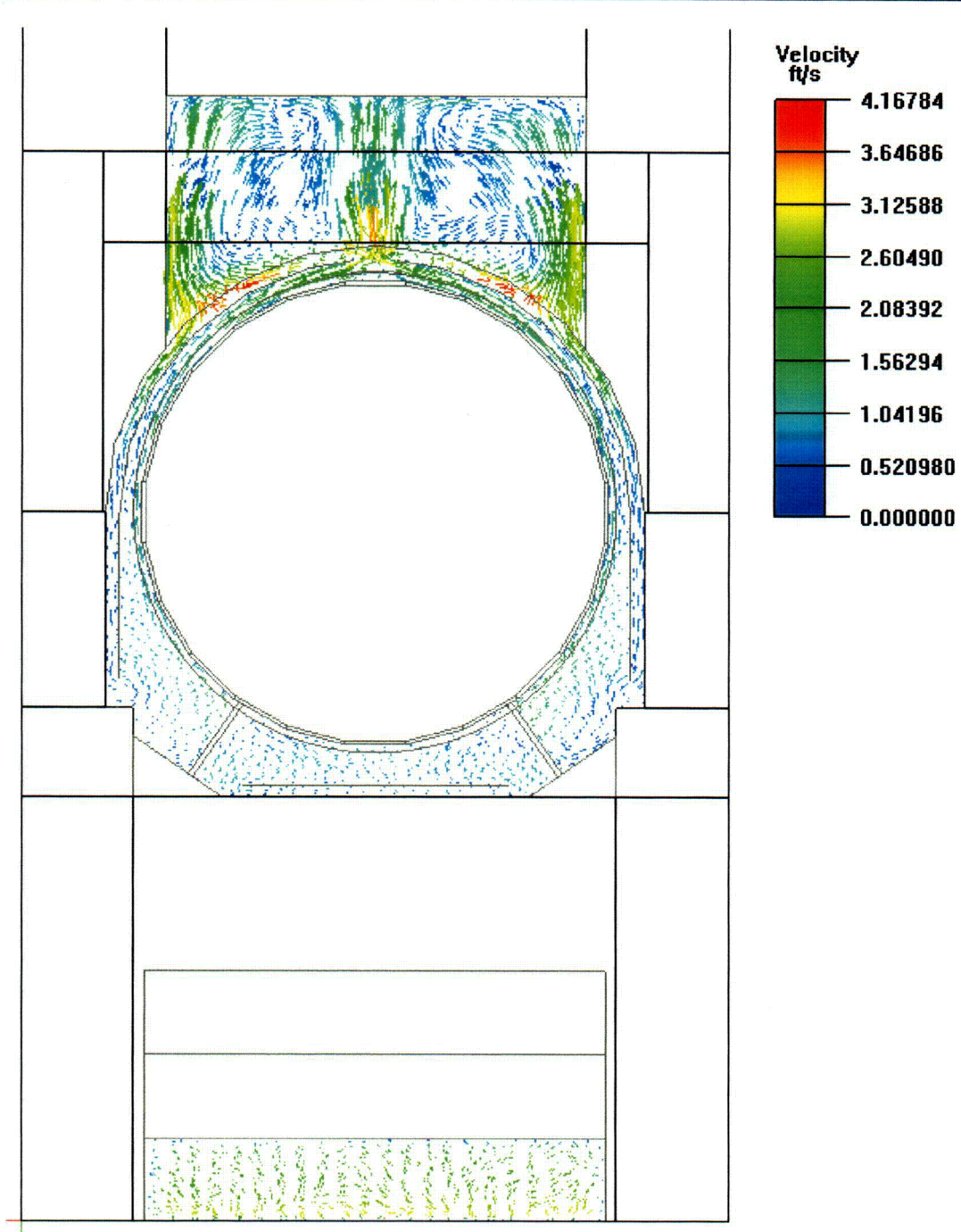


Figure 4-39 - Velocity Profile Along X-Y Plane Through AHSM, Off-Normal Cold Storage Condition

(Note: Cut plane approx. 8'-5" from front face of AHSM, i.e., through front vault duct)

C35

A TRANSCLEAR

PROJECT NO: SCE-23
CALCULATION NO: SCE-23.0410

REVISION: 2
PAGE: 58 of 65

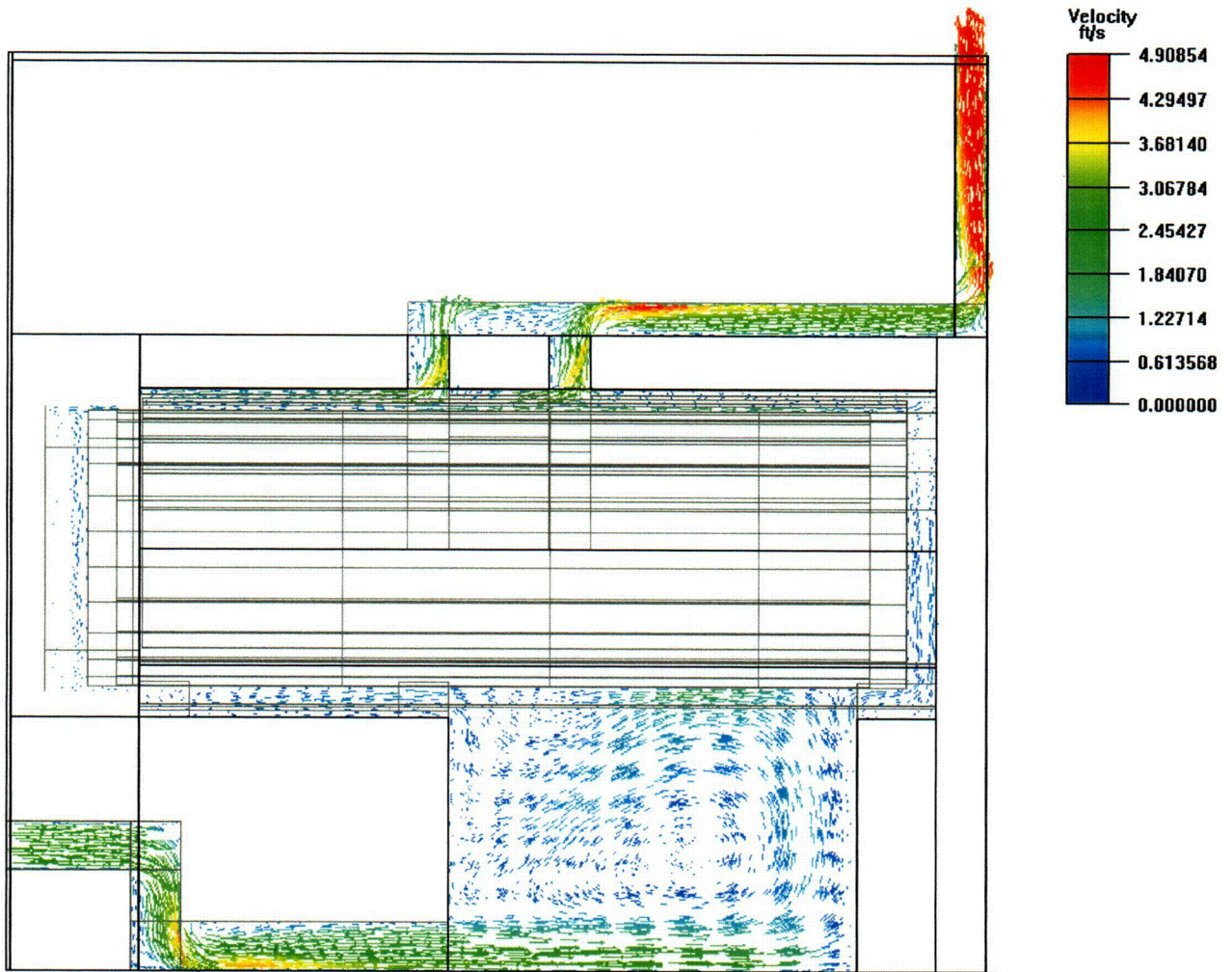


Figure 4-40 - Velocity Profile Along Y-Z Plane At Center Of AHSM, Off-Normal Cold Storage Condition

A TRANSNUCLEAR

PROJECT NO: SCE-23	REVISION: 2
CALCULATION NO: SCE-23.0410	PAGE: 59 of 65

5. SUMMARY AND CONCLUSION

A thermal analysis has been conducted on the prototypic thermal-hydraulic environment within the AHSM using a CFD methodology. The analysis examined the steady-state, design basis condition representing operations in a bounding normal hot day environment with a peak ambient temperature of 104°F, 24-hour averaged solar, and a DSC decay heat loading of 24 kW and the off-normal cold storage condition with an ambient air temperature of -40°F and no insolation. Table 5-1 presents a summary of peak temperatures predicted by this analysis for the normal hot condition of storage. For comparison, the temperatures presented in the Final Safety Analysis Report (FSAR, [6.1]) for the AHSM are also presented.

As can be seen from the table, the two analyses produce similar peak concrete temperature values and a similar air temperature rise through the module. The biggest difference between the two analysis approaches occurs for the predicted temperature distribution over the DSC shell surface and for the inner heat shield. This CFD based analysis predicts DSC shell temperatures that are 16 to 60°F hotter than the temperature levels presented in the FSAR, Rev. 0 [6.1]. The difference in predicted DSC shell temperatures is attributed primarily to the inability of the original FSAR methodology to account for the restricted airflow under the inner heat shield above the top of the DSC. The cooler temperatures noted from the CFD analysis at the DSC cover plates and shield plugs is directly related to the modeling approach used for this calculation where the decay heat from the fuel assemblies is applied to a 150" length of the DSC shell representing the active length of the fuel assemblies vs. applying the decay heat to the entire interior surface area of the DSC, as assumed by the [6.1] FSAR analysis. As such, the ends of the DSC received a direct heat load under the [6.1] FSAR analysis instead of only indirect heating via conduction from the shell, as assumed for this calculation.

Other than the DCS shell and inner heat shield temperatures, this evaluation finds that the [6.1] FSAR provides peak component temperatures that are similar or bounding to the temperatures produced using the CFD results.

Table 5-2 presents a summary of peak temperatures predicted by this analysis for the off-normal cold condition of storage. Again, the equivalent temperatures from Final Safety Analysis Report (FSAR, [6.1]) for the AHSM are also presented for comparison. Generally, the difference in the predicted temperatures between the two analyses is greater for the off-normal cold condition of storage than seen for the normal hot condition of storage presented in Table 5-1.

Table 5-3 presents the variation in the predicted DSC shell temperature vs. angular position on the DSC for the two analyzed storage conditions. These temperatures are taken from the axial section of the DSC with the highest peak temperature.

In conclusion, this calculation has developed and documented a thermal model of the AHSM based on a CFD methodology. That model has been used to evaluate the prototypic thermal-hydraulic environment within the AHSM for the bounding design basis hot day condition (i.e., the thermal condition producing the lowest thermal margin for the fuel cladding) and for the off-normal cold storage condition. The results demonstrate that the component temperatures are within their

A

TRANSNUCLEAR

PROJECT NO: SCE-23	REVISION: 2
CALCULATION NO: SCE-23.0410	PAGE: 60 of 65

associated limits of 800°F for stainless steels, 700°F for carbon steels, and 300°F for the concrete. The calculation also found that the [6.1] analysis provides peak concrete temperatures that are similar to the temperatures produced using the CFD based methodology of this calculation, but that the DSC shell and heat shield temperatures near the top of the module are under predicted by the [6.1] analysis. In addition, the CFD analysis indicates that the peak temperature gradient through the concrete is approximately 20% (i.e., $[80^{\circ}\text{F} - (-40^{\circ}\text{F})] / [56^{\circ}\text{F} - (-40^{\circ}\text{F})]$) higher than that predicted by the [6.1] FSAR analysis.

A TRANSNUCLEAR

PROJECT NO: SCE-23	REVISION: 2
CALCULATION NO: SCE-23.0410	PAGE: 61 of 65

Table 5-1 - Summary of Peak Component Temperatures For Normal Hot Storage

Component	Calculation Using CFD Methodology	Original FSAR Analysis	ΔT Between CFD & FSAR Methods
DSC Shell Top	459 °F	399 °F [Table 4.1-3, Ref. 6.1]	60 °F
DSC Shell Side	397 °F	---	---
DSC Shell Bottom	367 °F	351 °F [Table 4.4-3, Ref. 6.1]	16 °F
DSC Support Rail	281 °F	351 °F ¹ [Table 4.4-3, Ref. 6.1]	-70 °F
DSC Top Outer Cover Plate	204 °F	294 °F [Table 4.1-3, Ref. 6.1]	-90 °F
Inside Of DSC Top Shield Plug	218 °F		---
DSC Bottom Outer Cover Plate	231 °F	299 °F [Table 4.1-3, Ref. 6.1]	-68 °F
Inside Of DSC Bottom Shield Plug	254 °F		---
Inner Heat Shield	314 °F	258 °F [Table 4.1-3, Ref. 6.1]	57 °F
Upper Heat Shield	276 °F	258 °F [Table 4.1-3, Ref. 6.1]	18 °F
Concrete At Upper Back Wall	212 °F	219 °F [Table 4.1-3, Ref. 6.1]	-7 °F
Concrete At Roof Vault	232 °F	219 °F [Table 4.1-3, Ref. 6.1]	13 °F
Roof Outer Surface	212 °F	---	---
Avg. Roof Outer Surface	167 °F	---	---
Air Temperature Rise Thru Module	99 °F	96.4 °F [Table 4.4-1, Ref. 6.1]	2.6 °F
Airflow Mass Thru Module	0.85 lbm/sec	---	---

Table Notes: 1) Analysis does not specifically model the support structure, but assumes peak temperature is equal to the DSC shell temperature at the bottom

A TRANSNUCLEAR

PROJECT NO: SCE-23	REVISION: 2
CALCULATION NO: SCE-23.0410	PAGE: 62 of 65

Table 5-2 - Summary of Peak Component Temperatures For Off-Normal Cold Storage

Component	Calculation Using CFD Methodology	Original FSAR Analysis	ΔT Between CFD & FSAR Methods
DSC Shell Top	359 °F	271 °F [Table 4.4-5, Ref. 6.1]	88 °F
DSC Shell Side	276 °F	---	---
DSC Shell Bottom	278 °F	233 °F [Table 4.4-3, Ref. 6.1]	45 °F
DSC Support Rail	170 °F	233 °F ¹ [Table 4.4-3, Ref. 6.1]	-63 °F
DSC Top Outer Cover Plate	48 °F	166 °F [Table 4.1-3, Ref. 6.1]	-118 °F
Inside Of DSC Top Shield Plug	62 °F	---	---
DSC Bottom Outer Cover Plate	112 °F	174 °F [Table 4.1-3, Ref. 6.1]	-62 °F
Inside Of DSC Bottom Shield Plug	137 °F	---	---
Inner Heat Shield	180 °F	87 °F [Table 4.1-3, Ref. 6.1]	93 °F
Upper Heat Shield	136 °F	87 °F [Table 4.1-3, Ref. 6.1]	49 °F
Concrete At Upper Back Wall	61 °F	56 °F [Table 4.1-3, Ref. 6.1]	5 °F
Concrete At Roof Vault	80 °F	56 °F [Table 4.1-3, Ref. 6.1]	24 °F
Roof Outer Surface	51 °F	---	---
Avg. Roof Outer Surface	-14 °F	---	---
Air Temperature Rise Thru Module	80 °F	72.7 °F [Table 4.4-1, Ref. 6.1]	7.3 °F
Airflow Mass Thru Module	1.10 lbm/sec	---	---

Table Notes: 1) Analysis does not specifically model the support structure, but assumes peak temperature is equal to the DSC shell temperature at the bottom

A TRANSNUCLEAR

PROJECT NO: SCE-23	REVISION: 2
CALCULATION NO: SCE-23.0410	PAGE: 63 of 65

Table 5-3 - DSC Shell Temperatures vs. Circumferential Position

Angular Position on DSC (Bottom = 0°, Top = 180°)	DSC Shell Temperature, °F ¹	
	Normal Hot Storage ²	Off-Normal Cold Storage ³
0° to 7.5°	367.0	279.3
7.5° to 22.5°	368.6	278.0
22.5° to 37.5°	357.0	261.9
37.5° to 52.5°	357.3	253.1
52.5° to 67.5°	371.2	261.3
67.5° to 82.5°	385.9	263.0
82.5° to 97.5°	390.0	262.7
97.5° to 112.5°	388.4	268.9
112.5° to 127.5°	398.8	287.2
127.5° to 142.5°	417.8	310.8
142.5° to 157.5°	431.9	331.6
157.5° to 172.5°	447.1	346.2
172.5° to 180°	459.3	358.7

- Table Notes: 1) Indicated temperatures represent average of the shell temperatures from 0° to 180° with opposing counterparts from 180° to 360°.
 2) Temperatures for normal hot day condition with 104°F peak ambient and insolation.
 3) Temperatures for off-normal cold day condition with -40°F peak ambient and no insolation.

A TRANSNUCLEAR

PROJECT NO: SCE-23	REVISION: 2
CALCULATION NO: SCE-23.0410	PAGE: 64 of 65

6. REFERENCES

- 6.1 Final Safety Analysis Report, Standardized Advanced NUHOMS Horizontal Modular Storage System For Irradiated Nuclear Fuel, Transnuclear Inc., ANUH-01.0150, Revision 0, Docket Number 72-1029.
- 6.2 Drawings: NUHOMS[®] Advanced Horizontal Storage Module, NUH-03-.4011, Revision 2.
- 6.3 ASME Boiler & Pressure Vessel Code, Section II, Part D, Properties, 1998 Edition including 2000 addenda.
- 6.4 I.E. Idelchik, *Handbook of Hydraulic Resistance*, 3rd Edition, 1994.
- 6.5 *FLUENT[™]*, Version 6.1, Fluent, Inc., Lebanon, NH, 2003.
- 6.6 *ICEPAK[™]*, Version 4.1, Fluent, Inc., Lebanon, NH, 2003.
- 6.7 QA Validation and Verification Report #QA040.229.0001 For Software Codes FLUENT[™], Version 6.1, and ICEPAK[™], Version 4.1, Transnuclear, Inc., May 2004, Rev. 0.
- 6.8 "NUHOMS[®] Modular Spent-Fuel Storage System: Performance Testing", Report PNL-7327/UC-812/EPRI NP-6941, Pacific Northwest Laboratory & Carolina Power and Light Company, September 1990.
- 6.9 Rohsenow, Hartnett, and Choi, *Handbook of Heat Transfer*, 3rd edition, McGraw-Hill Publishers, 1998.

A

TRANSNUCLEAR

PROJECT NO:	SCE-23	REVISION:	2
CALCULATION NO:	SCE-23.0410	PAGE:	A1 of A1

APPENDIX A: FLUENT™ / ICEPAK™ RUN LOG

INTENTIONALLY LEFT BLANK